Geological Society of America
Special Paper 412
2006

Diverse volcanism in southeastern Guatemala: The role of crustal contamination

B.I. Cameron*
Department of Geosciences, University of Wisconsin, P.O. Box 413, Milwaukee, Wisconsin 53040, USA

J.A. Walker
Department of Geology and Environmental Geosciences, Davis Hall 312, Normal Road, DeKalb, Illinois 60115, USA

ABSTRACT

In the Central American arc, southeastern Guatemala hosts the most diverse volcanism. Large stratovolcanoes at the volcanic front (VF) form as a result of subduction of the oceanic Cocos plate beneath the continental Caribbean plate. Behind the volcanic front (BVF) volcanism, however, has undergone a fundamental change in eruptive style during the Quaternary from older, polygenetic central volcanism to younger, monogenetic cinder cone volcanism. Magmas that traverse the 40–45-km-thick crust in southeastern Guatemala are highly susceptible to crustal contamination. Consequently, mineral chemical data, whole-rock oxygen isotope, and light element geochemistry are used to investigate the relationship between edifice type and the magnitude of crustal contamination.

The lack of systematic variation between compositions of phenocryst phases and host rocks strongly suggests that open system processes were operating. Moreover, phenocryst core compositions are generally out of equilibrium with host rock compositions. Olivine from BVF cinder cones deviate only slightly from the equilibrium line in comparison to the older behind the volcanic front (OBVF) central volcanoes and VF stratovolcanoes, suggesting less assimilation of crustal lithologies. Steep arrays on the $\delta^{18}O$-SiO_2 diagram cannot be explained by crystal fractionation and favor the incorporation of ^{18}O-enriched crustal rocks. Higher $\delta^{18}O$ values in the OBVF central volcanoes and VF stratovolcanoes support the idea that larger, shallow magma bodies experienced greater amounts of crustal contamination. Regional extension in the Ipala Graben of southeastern Guatemala likely promoted short residence times in crustal reservoirs and small degrees of crustal assimilation for the BVF cinder cone magmas.

Keywords: Arc magmas, geochemistry, stable isotopes, crustal assimilation.

*E-mail: bcameron@uwm.edu

Cameron, B.I., and Walker, J.A., 2006, Diverse volcanism in southeastern Guatemala: The role of crustal contamination, *in* Rose, W.I., Bluth, G.J.S., Carr, M.J., Ewert, J., Patino, L.C., and Vallance, J., Volcanic hazards in Central America: Geological Society of America Special Paper 412, p. 121–139, doi: 10.1130/2006.2412(07).

INTRODUCTION

Magmatic systems can operate in an open or closed manner. Closed magmatic systems allow the exchange of heat with the system's surroundings, but not the exchange of mass. Open magmatic systems can exchange both energy and mass with their surroundings. Different volcanic edifice types in continental arcs result from enigmatic subvolcanic processes. In this paper, we try to ascertain whether open or closed systems processes predominated underneath arc volcanoes in southeastern Guatemala, using select geochemical data. For example, open system behavior, such as crustal assimilation, can change the chemical composition of a magma, including its critical volatile content. Volatile content drives explosive volcanic eruptions, which holds significant implications for the type of volcanic hazards to expect to be associated with the arc volcanoes.

The extent to which crustal contributions modify primary arc magmas remains a controversial issue amongst petrologists. Studies have convincingly demonstrated that crustal inputs play a significant role in the generation of evolved, high-SiO_2 continental arc lavas (Hildreth and Moorbath, 1988; Davidson et al., 1990; Feeley and Sharp, 1995). Greater uncertainty surrounds the contribution of the continental crust in less evolved basaltic arc lavas. In a single arc segment of northern Honshu, Japan, isotopic data for basalts vary systematically with changes in crustal lithology (Kersting et al., 1996). Apparently, even thin crustal lithosphere can modify the compositions of primary melts as they ascend from the mantle.

Although erupted through continental crust, the vast majority of Central American lavas show little evidence for pronounced crustal contamination, based on radiogenic isotopes (Walker et al., 1995; Feigenson et al., 2004). The relatively thin and young continental crust of southern Central America possesses distinct radiogenic isotopic characteristics compared to crust of most other continental margins. Consequently, if crustal assimilation occurs, it does not greatly influence the radiogenic isotopic compositions of the arc magma. The thickness of the continental crust in Central America peaks in western Guatemala at 48 km, from a minimum in Nicaragua of ~32 km (Carr, 1984). Crustal thicknesses decline in central and eastern Guatemala to 45 and 40 km, respectively (Carr et al., 1990). Therefore, Guatemalan lavas hold the most potential for registering crustal geochemical signatures. An unusual trend toward lower $^{206}Pb/^{204}Pb$ and more radiogenic $^{207}Pb/^{204}Pb$ and $^{208}Pb/^{204}Pb$ in southeastern Guatemala cinder cones could result from assimilation of granulitic crust (Walker et al., 1995). Southeastern Guatemala also hosts the most diverse arc volcanism in all of Central America and, consequently, warrants a detailed investigation of the role played by crustal contamination in creating diversity in magma compositions and edifice style.

GEOLOGICAL CONTEXT

Prominent stratovolcanoes or composite cones form a distinct line of volcanoes called the volcanic front (VF) in Guatemala (Fig. 1). The VF forms as a direct manifestation of subduction of the oceanic Cocos plate beneath the continental Caribbean plate. Common behind the volcanic front (BVF) volcanism adopts contrasting styles in southeastern Guatemala with time. Small composite cones were the site of polygenetic eruptions throughout the late Pliocene and are referred to as older behind the volcanic front (OBVF) central volcanoes. Ubiquitous cinder cones were erupted in proximity to the extensional Ipala Graben (Fig. 1) and locally developed on the flanks of the larger central volcanoes. These monogenetic volcanoes were accordingly assigned Quaternary ages (Walker, 1981). Shield volcanoes such as Las Viboras and calderas such as Retana and Ayarza were also constructed behind the front during the Quaternary (Fig. 1). Overall, however, BVF volcanism in southeastern Guatemala has undergone a fundamental change in eruptive style from older, polygenetic, central volcanism to younger, diffuse, monogenetic, cinder cone volcanism.

Conflicting ideas currently exist concerning the degree of crustal contamination expected to accompany different styles of arc volcanism. A specific plumbing system underlying one of the main edifice types in Guatemala may favor crustal assimilation over the others. In Mexico, as in Guatemala, the cinder cones represent small batches of magma that traverse a separate section of the crust only a single time (Hochstaedter et al., 1996). This eruptive character may make more differentiated members of the cinder cone suites more susceptible to crustal assimilation during their ascent to the surface. In sharp contrast, composite cones may erupt repeatedly through well-established plumbing systems. This feature suggests that older, crustally contaminated lavas may give way to larger volumes of magmas that were shielded in the conduit of the volcano from interacting with crustal rocks. Conversely, crustal contamination might flourish beneath composite cones where magma stalls in large crustal magma reservoirs. In Mexico, magmas erupted from cinder cones seem to experience more crustal contamination (Hochstaedter et al., 1996). In Guatemala, the appropriate data have not existed to test this hypothesis.

Detecting the geochemical signatures of crustal contamination depends not only on the degree of assimilation but also on the compositional contrast between magma and contaminant. Systematic increases in Sr isotopic ratios and decreases in Nd isotopic ratios across the arc in BVF cinder cones of Guatemala reflect either an absolute or apparent increase in crustal contamination (Walker et al., 1995; Feigenson et al., 2004). Absolute increases in crustal contamination associated with cinder cones from the Ipala Graben far behind the VF make geologic sense, if the normal faulting that accompanies extension facilitates assimilation by increasing the surface area of crustal lithologies. Alternatively, the extensional regime of eruption could result in less impedance and more direct access to the surface and, consequently, smaller degrees of contamination. In contrast, assimilation of equal amounts of older, more radiogenic crust in the Ipala Graben could also generate the observed isotopic changes. Low Nd isotopic ratios thought to represent crustal contamination were also measured in mafic lavas from Tegucigalpa in Honduras (Patino et al., 1997).

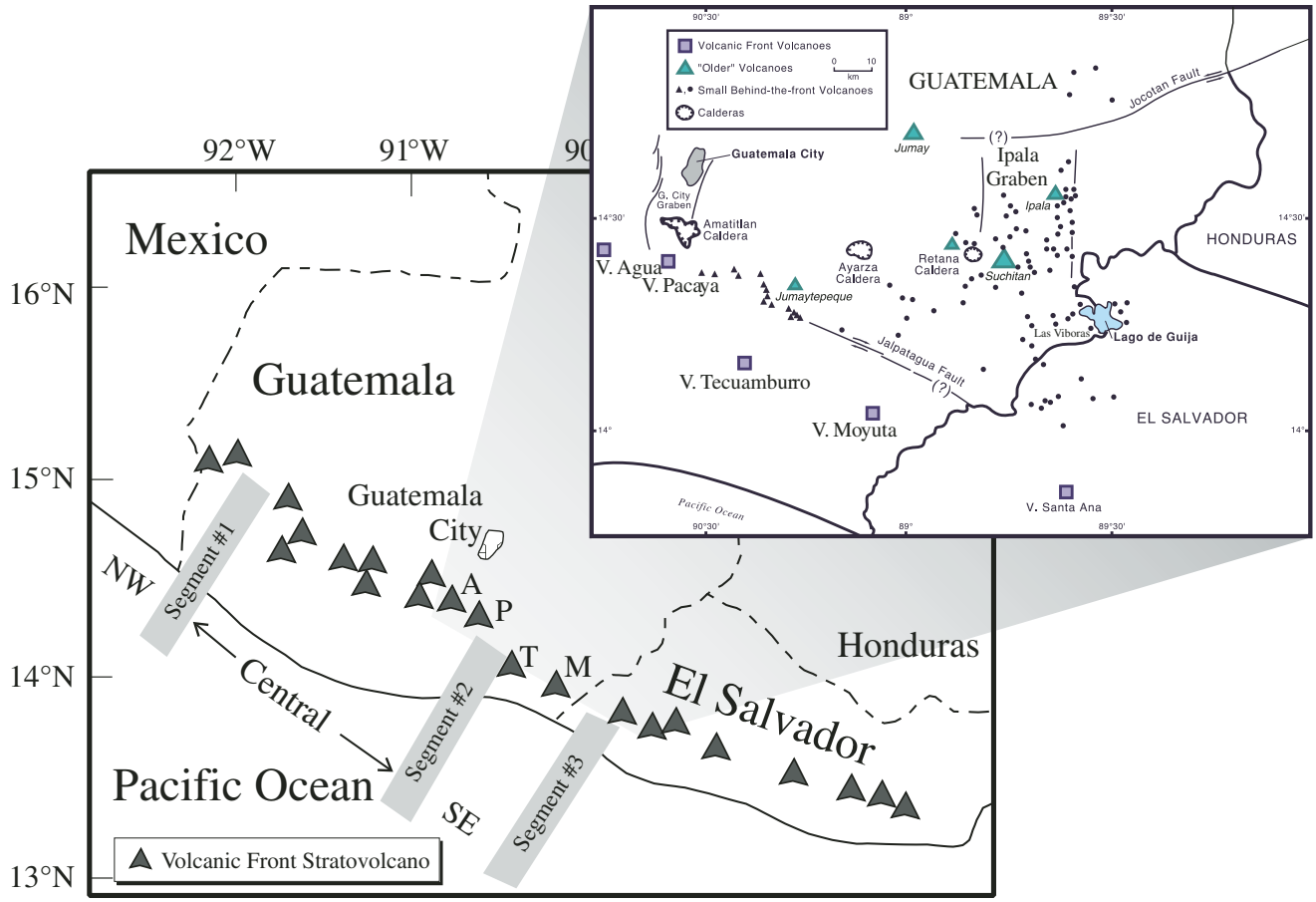

Figure 1. Location map for the three diverse groups of volcanoes examined in this geochemical study. The four volcanic front (VF) stratovolcanoes in southeastern Guatemala are Agua (A), Pacaya (P), Tecuamburro (T), and Moyuta (M). Segment #2 divides Agua and Pacaya from Tecuamburro and Moyuta. Inset: magnified view of the abundant behind the front volcanism (BVF) in southeastern Guatemala. Older BVF volcanism includes central volcanoes such as Ipala and Suchitan and calderas such as Retana and Ayarza. Younger BVF volcanism includes cinder cones that cluster in the Ipala Graben or along the trend of the Jalpatagua fault and shield volcanoes such as Las Viboras near Lago de Guija on the border with El Salvador.

Nd isotopic ratios remain rather uniform throughout the Central American arc except for samples from western Guatemala (Fig. 2A). Here, low Nd isotopic ratios occur in VF lavas that traverse the thickest section of crust (Carr et al., 1990). The erratic behavior of Rb/Nd ratios (Fig. 2B) in volcanic rocks from Guatemala compared to other segments of the arc suggests differing petrogenetic processes. The lower Nd isotopic values and higher Rb/Nd ratios of the VF lavas yield the first order suggestion that the composite cones possess greater degrees of crustal contamination.

GEOCHEMICAL APPROACH

Examination of relationships between mineral phases and the whole-rock composition lends qualitative information on the petrological evolution of shallow magma chamber systems (Sakuyama, 1981; Hunter and Blake, 1995). Moreover, assimilation of granites and other crustal rocks in Mexico has been shown to enrich differentiated arc lavas in boron (B) (Hochstaedter et al., 1996). In addition, oxygen isotope data on whole-rocks and mineral separates can potentially supply unequivocal evidence of crustal inputs to arc magmas (Ellam and Harmon, 1990; Davidson et al., 1990; Feeley and Sharp, 1995; Pokrovskii and Volynets, 1999) and also provide an excellent means of quantifying the role of the continental crust as a magmatic source (Smith et al., 1996; Harmon and Gerbe, 1992). Thus, in an attempt to augment our limited knowledge on the extent of crustal contamination in Central American lavas, we discuss in this paper mineral composition, whole-rock oxygen isotope, and elemental B, Be, and Li data for lavas erupted in southeastern Guatemala.

SAMPLES AND METHODS

Representative samples of VF stratovolcanoes, OBVF central volcanoes, and BVF cinder cones were selected for the mineral chemical study. The chemical compositions of groundmass

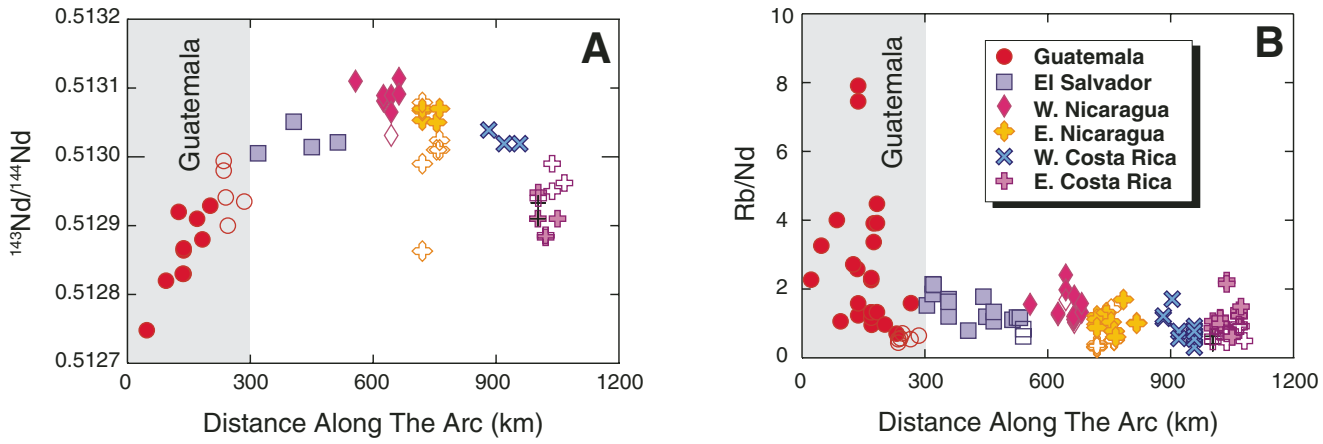

Figure 2. Variations in mafic samples along the Central American arc in geochemical parameters that indicate crustal contamination is most likely in southeastern Guatemala. (A) Low $^{143}Nd/^{144}Nd$ occurs in Guatemala (circles). Behind the volcanic front (BVF) volcanism is shown by open circles. Crustal contamination or anomalous mantle may explain the complementary low $^{143}Nd/^{144}Nd$ in Costa Rica (crosses). (B) Guatemalan lavas possess high Rb/Nd ratios compared to the rest of the Central American arc.

and phenocryst phases were measured with a Cameca SX-50 electron microprobe at the University of Chicago, calibrated with natural and synthetic standards. The program audit profile (PAP) correction routine was utilized for all analyses. Typical analytical conditions adopted were a 15 kV accelerating voltage and a 25 nA beam current. Most analyses were run with a focused beam and a beam width of 1–2 µm. Tables 1–3 report representative major element compositions and mineral formulae of olivine, pyroxene, and plagioclase.

Significant crustal inputs of the light elements (i.e., Li, Be, and B) to arc magmas seem especially probable where granitoid rocks serve as the contaminant. Consequently, the light elements were measured on a subset of 23 lavas from southeast Guatemala and two possible crustal contaminants by direct current plasma atomic emission spectrometry (DCP-AES) using an ARL model SpectraSpan (SS) 7 DCP at the University of South Florida. Three standards were run for B (RR-1, NBS-688, and QDF-1), and two standards (STM-1 and QLO-1) were analyzed for Li and Be to

TABLE 1. REPRESENTATIVE OLIVINE MINERAL CHEMICAL DATA

Sample	GIP.1Pc*	GIP.1Pr	GIP.1GM	GCC837.Pc	GCC837.Pr	GCC837.GM	G201.GM	T302.Pc	T302.Pr
Group	OBVF	OBVF	OBVF	BVF	BVF	BVF	BVF	VF	VF
SiO_2	37.08	34.19	34.79	39.62	38.14	37.06	36.53	39.07	37.96
MgO	34.35	22.35	23.59	41.12	36.18	31.15	29.32	41.51	35.32
FeO	27.16	41.76	40.34	18.53	24.34	30.49	32.82	18.28	25.24
MnO	0.42	0.89	0.78	0.22	0.48	0.63	0.73	0.23	0.42
CaO	0.19	0.3	0.29	0.15	0.2	0.35	0.33	0.13	0.16
NiO	0.05	0.05	0	0.02	0.03	0.05	0.08	0.07	0.06
Total	99.25	99.54	99.79	99.66	99.37	99.73	99.81	99.29	99.16
Formula based on 4 oxygens									
Si	0.998	0.993	0.998	1.013	1.009	1.008	1.006	1.004	1.011
Mg	1.378	0.968	1.009	1.568	1.427	1.264	1.204	1.59	1.402
Fe	0.611	1.014	0.968	0.396	0.538	0.694	0.756	0.393	0.562
Mn	0.01	0.022	0.019	0.005	0.011	0.015	0.017	0.005	0.009
Ca	0.005	0.009	0.009	0.004	0.006	0.01	0.01	0.004	0.005
Ni	0.001	0.001	0	0	0.001	0.001	0.002	0.001	0.001
mol% end members									
Fo	69.3	48.8	51.0	79.8	72.6	64.6	61.4	80.2	71.4
Fa	30.7	51.2	49.0	20.2	27.4	35.4	38.5	19.8	28.6

Note: BVF—behind the volcanic front; OBVF—older behind the volcanic front; VF—volcanic front.
*The prefix of the sample designations stands for Guatemala and the particular volcano, whereas the suffix is composite of texture (eg. P—phenocryst, GM—groundmass) and analysis location (eg. c—core or r—rim).

assess precision and accuracy. Results of other studies quote errors within 10% (relative) of accepted values for both B and Be (Hochstaedter et al., 1996). In this study, precision for B was closer to 20% at the 1 ppm level, but improved to ~1% at the 10 ppm level. Errors on the Be standards were 11 and 16% at the 1 ppm and 10 ppm level, respectively. Li analyses had errors between 0.06% and 4.1%. Table 4 presents the new Li, Be, and B data.

Oxygen-isotopic ratios were determined on ~12 mg samples of 27 separate whole-rock powders at the Stable Isotope Laboratory at Southern Methodist University in Dallas. Oxygen was extracted from powders following reaction with ClF_3. Typical analytical precision on whole-rock $\delta^{18}O$ values approximated ±0.2‰ based on standards and repeat analyses. Of the whole-rock powders analyzed, two are crustal rocks, seven are lavas from VF stratovolcanoes, nine are from OBVF central volcanoes, and nine are from BVF cinder cones. Table 4 also reports the analytical results in the standard per mil (‰) notation as deviations relative to the standard mean ocean water (SMOW) standard.

RESULTS

Mineral Chemical Data

Olivine occurs as a phenocryst and groundmass phase in basalts and basaltic andesites in southeast Guatemala (Table 1). Normal zoning displayed by backscatter images was confirmed by electron microprobe analyses. Olivine cores (Fig. 3A; mean $Fo_{73.1}$) are generally more enriched in Mg relative to rim compositions (Fig. 3B; mean $Fo_{64.5}$). Groundmass olivine grains (mean $Fo_{56.2}$) are more Mg-poor than both phenocryst cores and rims (Fig. 3C).

A comparison of olivine compositions at the different edifice styles shows that olivine cores at VF composite cones (mean

TABLE 2. REPRESENTATIVE PYROXENE MINERAL CHEMICAL DATA

Sample	GJM.2Pc*	GJM.2Pr	GJM.2GM	GCC911.GM	GCC837.Pc	T302.Pc	T302.Pr	M210.Pc	M210.Pr
Group	OBVF	OBVF	OBVF	BVF	BVF	VF	VF	VF	VF
SiO_2	52.2	51.78	49.35	52.57	48.36	50.76	51.9	51.62	51.04
Al_2O_3	2.15	1.92	3.68	1.51	4.29	4.09	2.94	2.03	2.1
Fe_2O_3	2.06	2.47	2.85	0	3.46	1.5	0.43	0.11	0.1
TiO_2	0.42	0.39	1.48	0.57	1.48	0.7	0.54	0.5	0.52
Cr_2O_3	0.01	0	0.09	0.18	0.06	0.03	0.03	0.01	0.01
MgO	24.67	24.74	14.47	17.06	12.96	14.89	15.22	13.79	13.09
FeO	15.92	15.27	7	11.85	8.4	7.32	8.53	11.66	10.72
MnO	0.38	0.44	0.24	0.4	0.29	0.23	0.29	0.4	0.4
CaO	1.84	1.75	19.87	15.06	20.02	20	19.73	18.57	19.63
Na_2O	0.03	0.03	0.37	0.2	0.38	0.34	0.27	0.37	0.41
Total	99.68	98.79	99.4	99.4	99.7	99.86	99.88	99.06	98.02
Formula based on 6 oxygens									
Si	1.915	1.915	1.85	1.96	1.826	1.882	1.925	1.953	1.951
Al	0.085	0.084	0.15	0.04	0.174	0.118	0.075	0.047	0.049
Fe^{3+}	0	0.001	0	0	0	0	0	0	0
Al	0.008	0	0.013	0.026	0.017	0.061	0.054	0.044	0.046
Fe^{3+}	0.057	0.068	0.08	0	0.098	0.42	0.012	0.003	0.003
Ti	0.012	0.011	0.042	0.016	0.042	0.2	0.015	0.014	0.015
Cr	0	0	0.003	0.005	0.002	0.001	0.001	0	0
Mg	0.923	0.921	0.809	0.948	0.729	0.823	0.841	0.778	0.746
Fe^{2+}	0	0	0.053	0.005	0.112	0.053	0.077	0.161	0.19
Mn	0	0	0	0	0	0	0	0	0
Mg	0.426	0.443	0	0	0	0	0	0	0
Fe^{2+}	0.488	0.472	0.166	0.365	0.153	0.174	0.188	0.208	0.153
Mn	0.012	0.014	0.008	0.013	0.009	0.007	0.009	0.013	0.013
Ca	0.072	0.069	0.798	0.602	0.81	0.795	0.784	0.753	0.804
Na	0.002	0.002	0.027	0.014	0.028	0.24	0.019	0.027	0.03
mol% end members									
Wo	3.8	3.6	43.7	31.3	44.9	43.1	41.5	39.6	42.5
En	70.7	71.6	44.3	49.4	40.4	44.6	44.5	41.0	39.4
Fs	25.6	24.8	12.0	19.3	14.7	12.3	14.0	19.4	18.1

Note: BVF—behind the volcanic front; OBVF—older behind the volcanic front; VF—volcanic front.
*The prefix of the sample designations stands for Guatemala and the particular volcano, whereas the suffix is composite of texture (eg. P—phenocryst, GM—groundmass) and analysis location (eg. c—core or r—rim).

TABLE 3. REPRESENTATIVE PLAGIOCLASE MINERAL CHEMICAL DATA

Sample	GJM.2Pc	GJM.2Pr	GJM.2GM	GCH.1GM	GCC837.Pc	GCC837.Pr	GCC837.GM	T302.Pc	T302.Pr
Group	OBVF	OBVF	OBVF	OBVF	BVF	BVF	BVF	VF	VF
SiO_2	52.86	51.22	54.14	52.89	46.63	49.71	49.73	45.08	49.5
Al_2O_3	28.78	30.24	27.7	29.08	33.48	30.69	31.37	34.35	31.3
Na_2O	4.47	3.48	5.08	4.37	1.59	3.07	2.85	1.27	3.07
CaO	12.18	13.96	11.02	12.07	17.43	14.77	15.13	17.64	14.79
K_2O	0.25	0.18	0.34	0.34	0.05	0.15	0.13	0	0.06
BaO	0	0	0	0.04	0	0	0	0	0
Total	98.54	99.08	98.28	98.79	99.18	98.39	99.21	98.34	98.72
Formula based on 32 oxygens									
Si	9.713	9.401	9.945	9.694	8.64	9.217	9.147	8.435	9.145
Al	6.233	6.542	5.998	6.282	7.312	6.707	6.801	7.576	6.816
Na	1.593	1.238	1.809	1.553	0.571	1.104	1.016	0.461	1.1
Ca	2.398	2.745	2.169	2.37	3.461	2.935	2.982	3.537	2.928
K	0.059	0.042	0.08	0.08	0.012	0.035	0.031	0	0.014
Ba	0	0	0	0.003	0	0	0	0	0
mol% end members									
Ab	39.3	30.8	44.6	38.8	14.1	27.1	25.2	11.5	27.2
An	59.2	68.2	53.4	59.2	85.6	72.0	74.0	88.5	72.4

Note: BVF—behind the volcanic front; OBVF—older behind the volcanic front; VF—volcanic front.
*The prefix of the sample designations stands for Guatemala and the particular volcano, whereas the suffix is composite of texture (eg. P—phenocryst, GM—groundmass) and analysis location (eg. c—core or r—rim).

TABLE 4. OXYGEN AND Sr ISOTOPIC DATA ALONG WITH SELECT TRACE ELEMENTS

Sample	Group	SiO_2 (wt%)	$\delta^{18}O$ (‰)	$^{87}Sr/^{86}Sr^{\dagger}$	B (ppm)	Be (ppm)	Li (ppm)	La (ppm)	Pb (ppm)	Th (ppm)	Cs (ppm)	U (ppm)	Rb (ppm)	Sb (ppm)	Ba (ppm)
G2	Crust	59.65	3.71	0.7066	24.1	1.13	21.7	21.21	14.88	8.43	0.39	1.26	1.33	66.02	497.3
M2	Crust	81.19	14.27	0.74277	22.0	0.45	1.9	34.1	5.76	6.78	5.612	1.773			1377
GUC-201	BVF	50.36	6.47	0.703547				12.53	5.17	1.25	0.53	0.53	14.12	0.17	404.8
GUC-911	BVF	53.71	7.74	0.704054	9.9	1.29	9.0	28.53	7.14	1.19	0.6	0.5	25.12	0.1	1039
GUC-837	BVF	49.01	6.61	0.703975	2.3	0.87	7.8	14.05	5.25	0.96	0.39	0.41	17.41	0.09	344.4
GUC-839	BVF	48.32	6.7					11.73	3.58	0.82	0.16	0.34	7.94	0.03	263.6
GUC-844	BVF	50.39	6.63	0.703791	2.7	1.07	8.4	14.21	4.9	1.48	0.27	0.64	23.31	0.05	462.2
GUC-702	BVF	49.98	6.72	0.70353	2.7	1.33	9.2	15.18	4.1	1.07	0.24	0.5	13.6	0.02	402.2
GUC-800	BVF	48.76	6.16		1.1	0.85	7.4	10	2.59	0.95	0.15	0.22	7.33		248.3
GUC-25	BVF	53.7		0.70381	10.0	1.66	12.3	26	6.6	2.07	0.26	0.82	20.88	0.05	624.7
GUC-303	BVF	49.9		0.70321	4.0	0.92	7.3	9	2.25	0.67	0.04	0.17	6.64		181.4
GUAT-20	BVF		6.67												
GUAT-33	BVF		6.98												
GUC-835	OBVF	50.33	6.87	0.70415				15.13	4.85	1.13	0.37	0.53	17.65	0.05	500.5
GSU-01	OBVF	52.56	7.5	0.704135	8.3	0.86	9.4	12	6.71	1.89	1.09	0.69	36.77	0.17	470.6
GSU-04	OBVF	55.43	7.41	0.704101	4.5	1.24	9.2	22.88	8.91	3.1	1.41	1.22	50.99	0.13	668.2
GIP-01	OBVF	52	7.14	0.703877	4.1	1.36	10.0	18.6	6.45	1.93	0.83	0.78	29.92	0.17	504.8
GIP-04	OBVF	51.04	7.12	0.703884	2.6	0.87	8.6	15.13	4.43	1.47	0.35	0.63	18.96	0.07	480.8
GJM-02	OBVF	56.67	7.86		11.5	1.08	17.3	21.74	7.64	3.9	1.38	1.26	47.37	0.15	676.9
GJM-03	OBVF	51.73	7.85		6.8	0.76	11.5	12.64	4.97	2.04	0.89	0.68	26.93	0.11	480.7
GCH-01	OBVF	51.15	6.9		2.6	1.01	10.0	20.08	4.47	1.47	0.67	0.61	17.33	0.08	582.2
GUC-812	OBVF	49.91	6.51		3.7	0.98	8.4	16.04	4.39	1	0.12	0.28	9.77	0.02	354.2
LC-2	OBVF	54.75		0.704102	8.0	1.16	10.1	23.49	7.98	2.28	0.78	0.78	38.61	0.18	865.8
FEL-3	OBVF	58.25		0.70409	18.1	1.23	11.4	23.35	12.1	3.01	0.73	1.04	54.22	0.3	935.9
FVH-4	OBVF	64.32		0.704056	22.8	1.33	10.4	25.61	13.6	5.02	2.32	1.83	99.48	0.39	943
GPA-01	VF	49.26	6.36					8.2	3.26	0.96	0.41	0.42	10.26	0.02	341.2
GAG-21	VF	51.4	6.59		6.0	0.75		10.48	5.49	1.57	0.62	0.67	19.53	0.2	519.9
GAG-27	VF	55.31	6.79					13.19	5.07	2.21	0.6	0.99	39.69	0.25	638.1
GAG-10	VF	59.1	6.78					16.09	8.12	3.17	1.93	1.46	55.92	0.4	748.7
TCB-302	VF	53.87	6.73					5.83	3.27	0.45	0.77	0.25	9.41	0.54	314.7
E1	VF	51.4	7.44	0.70389	3.1	0.62	9.2	10.15	5.51	1.47	0.58	0.58	13.53		442.3
GMO-201	VF	57.46	8.41	0.703649	22.9	0.78	9.6	12.29	8.12	3.43	2.11	1.48	46.59	0.7	669
Qam-13	VF	49.81			7.0	0.58	9.2	8.51	4.6	1.87	0.64	0.62	13.6		486.6

Note: BVF—behind the volcanic front; OBVF—older behind the volcanic front; VF—volcanic front.
†Sr isotopic ratios were obtained at the mass spectrometry facility at Rutgers University. Sr isotopic ratios are normalized to $^{86}Sr/^{88}Sr$ of 0.1194 and are reported as measured.

$Fo_{75.3}$; Fig. 3A) and BVF cinder cones (mean $Fo_{76.0}$; Fig. 3A) have slight enrichments in Mg compared to the OBVF central volcanoes (mean $Fo_{71.6}$; Fig. 3A). Moreover, VF stratovolcanoes and BVF cinder cones have more narrow ranges of olivine core compositions (Fig. 3). In contrast, OBVF central volcanoes contain olivine that extends the range in forsterite (Fo) content to below 60 mol% (Fig. 3).

Clinopyroxene occurs as both a phenocryst and groundmass phase in most lavas from southeast Guatemala, except for BVF cinder cones, which only contain clinopyroxene as a groundmass phase. In contrast to olivine, backscatter images and electron microprobe analyses showed little chemical zoning in the clinopyroxene phenocrysts. Phenocryst cores (Fig. 4A; mean Mg number = 77.0) have nearly identical ranges and means as phenocryst rims (Fig. 4B; mean Mg number = 77.4). Groundmass clinopyroxene grains possess a similar range in Mg number as phenocrysts (Fig. 4C), but have a slightly lower average value (mean Mg number = 74.2). More evolved samples, such as the dacite (Figs. 4A and 4B), display both normal and reversed zoning, though variations in Mg number are relatively small. Clinopyroxene compositions vary little as whole-rock SiO_2 increases.

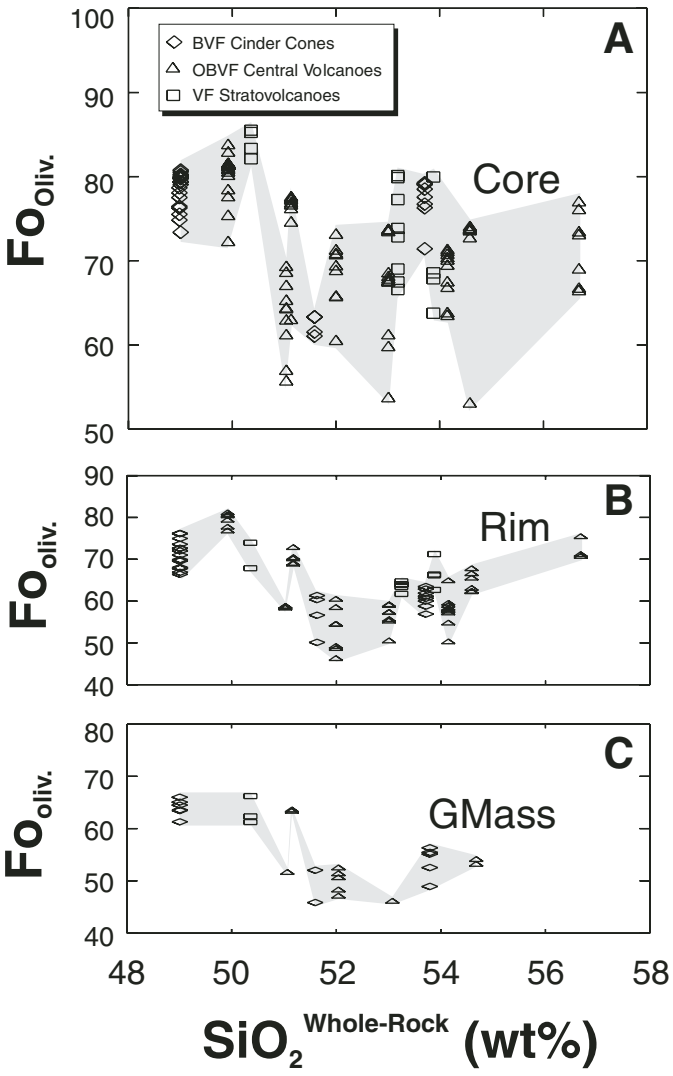

Figure 3. Forsterite (Fo) content variations in olivine against whole rock SiO_2 compositions. (A) Core Fo contents in olivine phenocrysts. (B) Rim Fo contents in olivine phenocrysts. (C) Groundmass (GMass) olivine Fo contents. Shaded compositional envelopes were drawn to highlight that little systematic variation exists between the Fo contents and the host rock chemistry.

Clinopyroxene core compositions at VF stratovolcanoes (mean Mg number = 77.0) and OBVF central volcanoes (mean Mg number = 77.0) have similar ranges (Fig. 4A) and an identical mean. Owing to the paucity of clinopyroxene phenocrysts in cinder cone lavas, only one phenocryst core was measured in a BVF cinder cone rock, and its Mg# is 73.3 (Fig. 4A). The range for groundmass clinopyroxene in BVF cinder cones is shifted to lower Mg numbers (62.2–80.8) relative to the phenocrysts in lavas from the other edifice types (Fig. 4). The mean Mg number of the groundmass clinopyroxene at BVF cinder cones (Mg number = 72.7) is lower than the clinopyroxene phenocryst core and rim compositions from the other edifice types, but approximates the mean from the lone phenocryst analysis from a Guatemalan cinder cone (Fig. 4A).

Orthopyroxene occurs in lower modal abundances as phenocryst and groundmass phases than clinopyroxene in most Guatemalan lavas. Groundmass and phenocryst orthopyroxene exhibit a similar range of compositions (Fig. 5). Moreover, orthopyroxene phenocryst cores, rims, and groundmass grains have nearly identical mean Mg numbers (mean Mg number of 71.9, 70.9, and 70.3, respectively). Despite these similar means, the data show both normal and reversely zoned phenocrysts in some of the more evolved magmas. It is noteworthy that Mg-rich cores persist across the compositional spectrum. The lower Mg number of orthopyroxene cores (mean Mg number = 71.9) compared to clinopyroxene (mean Mg number = 77.0) in the lavas from southeast Guatemala may indicate that orthopyroxene occurs later in the crystallization history.

Slight variations in orthopyroxene core composition exist based on the type of volcanic edifice (Fig. 5). Although orthopyroxene phenocrysts from OBVF central volcanoes and VF stratovolcanoes have similar ranges in Mg number (Fig. 5A), orthopyroxene cores in lavas from the former edifice type (mean Mg number = 73.1) have a higher mean Mg number than the latter (mean Mg number = 70.2). No orthopyroxene phenocrysts from BVF cinder cones were analyzed by the electron microprobe.

Plagioclase occurs as a modally abundant phenocryst and groundmass phase in the arc lavas of southeast Guatemala. Both phenocryst cores and rims exhibit a nearly identical, wide range of An contents (Figs. 6A and 6B), yet generally display normal zoning. The mean An values for plagioclase phenocryst cores and rims ($An_{70.5}$ and $An_{61.6}$, respectively) reflects the predominance of normally zoned crystals. However, some more-evolved samples

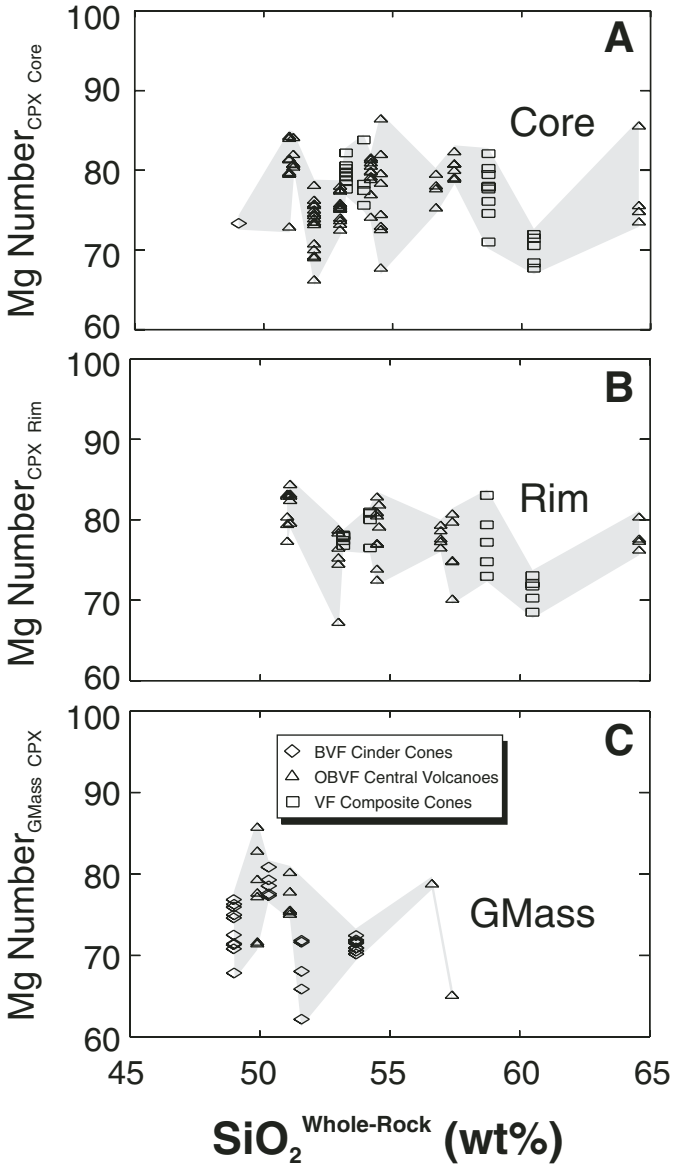

Figure 4. Mg number variations in clinopyroxene grains versus whole-rock SiO_2 compositions. (A) Core Mg number values of clinopyroxene phenocrysts. (B) Rim Mg number values of clinopyroxene phenocrysts. (C) Mg number contents of groundmass (GMass) clinopyroxene grains. Shaded compositional envelopes were drawn to highlight the nonsystematic relationship between Mg number in clinopyroxene versus host rock composition.

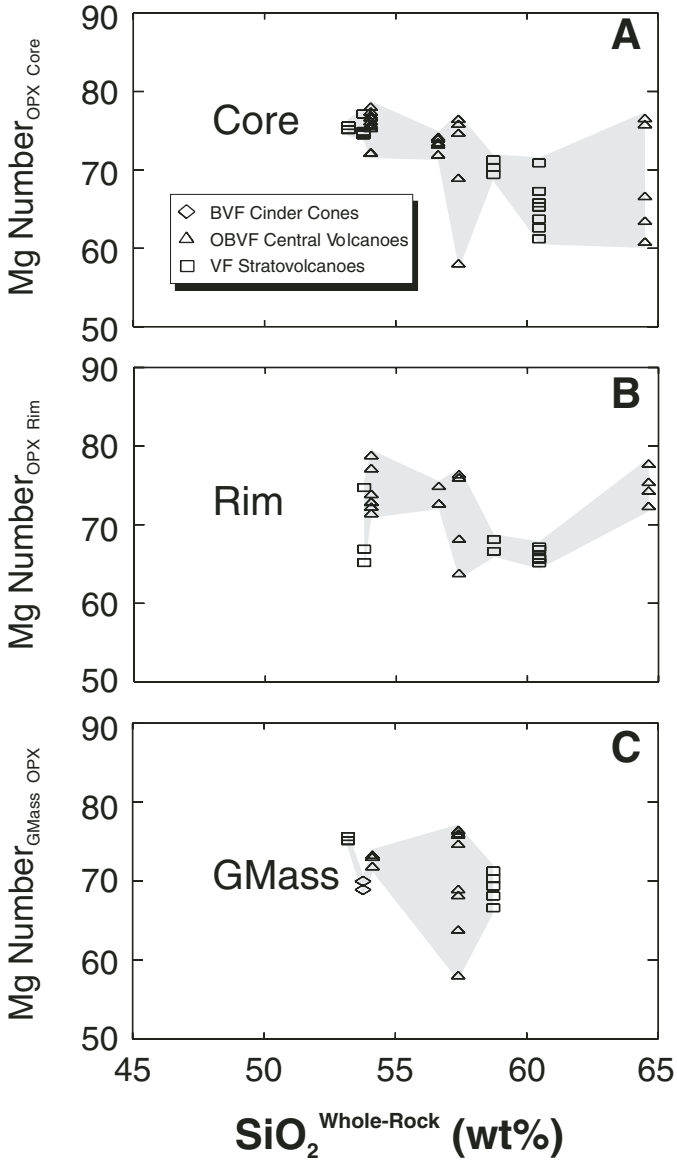

Figure 5. Mg number variations in orthopyroxene grains versus whole-rock SiO_2 compositions. (A) Mg number values for orthopyroxene phenocrysts. (B) Rim Mg number values of orthopyroxene phenocrysts. (C) Mg number values for groundmass (GMass) orthopyroxene. Shaded compositional envelopes were drawn to highlight that Mg number in orthopyroxene remains relatively constant over a range of host rock SiO_2 compositions.

do display both normal and reversed zoning. A lower mean An content in groundmass plagioclase (mean $An_{58.6}$) relative to phenocryst rims (mean $An_{61.6}$) continues the overall shift in the range of An contents to lower values with inferred crystallization order. An content in plagioclase crystals varies considerably at whole-rock SiO_2 contents <57 wt%, but generally decreases at SiO_2 contents >57% wt% (Figs. 6A and 6B).

Plagioclase crystals of varying composition occur in lavas erupted from the different edifice types (Fig. 6). Plagioclase cores from polygenetic VF stratovolcanoes and OBVF central volcanoes exhibit large ranges in An content (Fig. 6A), whereas those from monogenetic BVF cinder cones display a more narrow range toward the high end of the An spectrum (Fig. 6A). The mean An content of plagioclase phenocryst cores from BVF cinder cones is substantially higher (mean $An_{74.9}$) than those from VF stratovolcanoes (mean $An_{64.5}$) or OBVF central volcanoes (mean $An_{70.8}$). The same pattern of An variation occurs amongst plagioclase rim compositions (Fig. 6B).

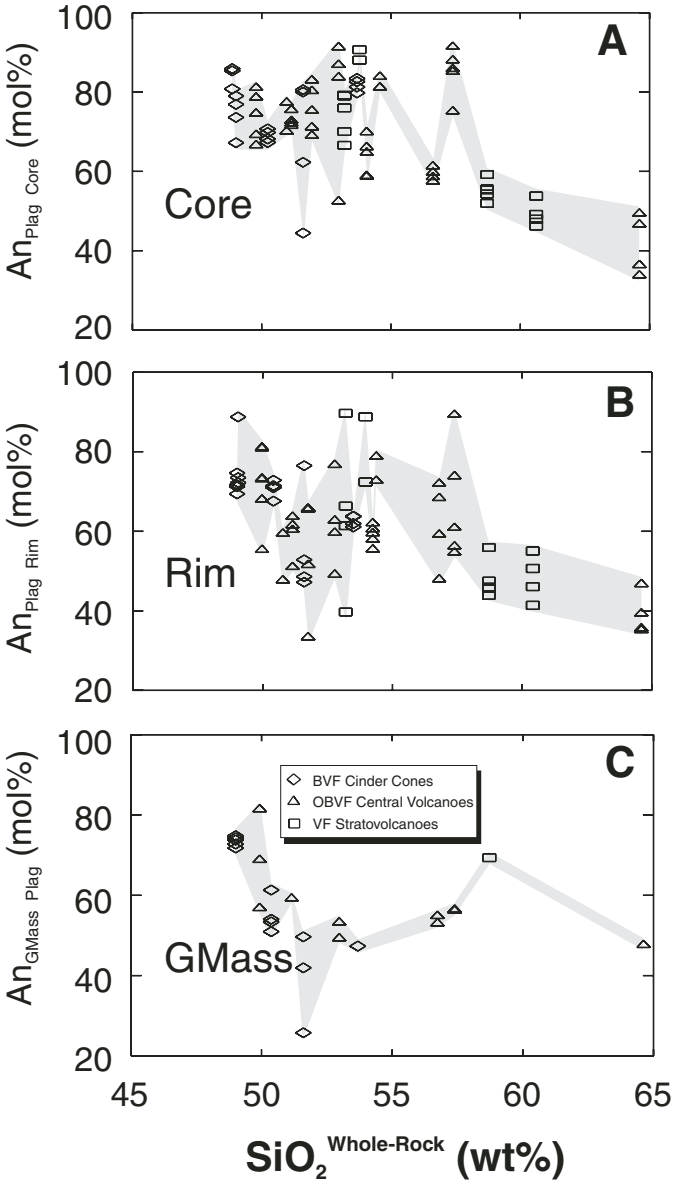

Figure 6. An content variations in plagioclase crystals versus whole-rock SiO_2 compositions. (A) Core An contents of plagioclase phenocrysts. (B) Rim An contents of plagioclase phenocrysts. (C) An contents of groundmass (GMass) plagioclase. Shaded compositional envelopes show no relationship between An content and host rock composition.

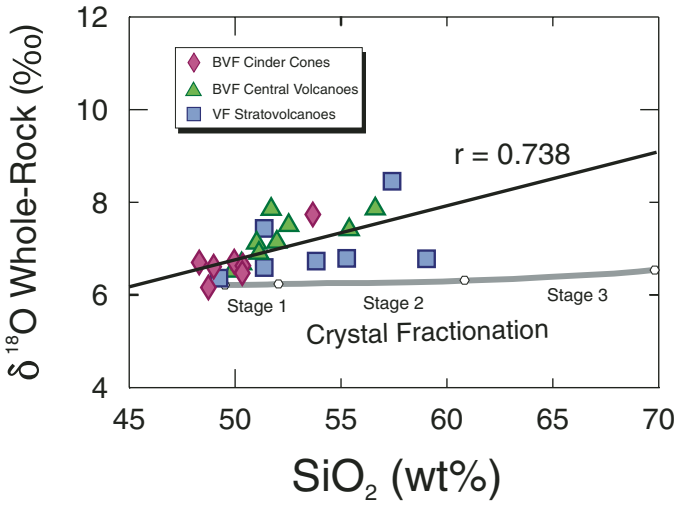

Figure 7. $\delta^{18}O_{whole\text{-}rock}$ versus SiO_2 diagram. $\delta^{18}O$ correlated positively with SiO_2, with a Spearman rank correlation coefficient of +0.738. The relatively steep positive trend of the Guatemalan arc lavas contrasts with the near-horizontal crystal fractionation trend. Owing to the large range of compositions found at subduction zone volcanoes (i.e., from rhyolite to basalt), the crystal fractionation trend was modeled in three different stages. Stage 1, 2, and 3 refers to least squares mixing crystal fractionation models. See text for details. Behind the volcanic front (BVF) cinder cone lavas have lower $\delta^{18}O$ values than both volcanic front (VF) stratovolcanoes and older behind the volcanic front (OBVF) central volcanoes.

Oxygen Isotopic Compositions

The whole-rock oxygen isotope data from southeastern Guatemala span a wide range for young, fresh arc lavas (6.16–8.46‰). Basalts associated with subduction at convergent margins show enrichments in whole-rock $\delta^{18}O$ relative to mid-oceanic-ridge basalt (MORB) ($\delta^{18}O$ = +5.7‰). Forearc trough and backarc basin basalts have a mean $\delta^{18}O$ of 5.9‰; oceanic arc basalts have a mean $\delta^{18}O$ of 6.0‰; and continental arc basalts average 6.2‰ (Harmon and Hoefs 1995). Oxygen isotope analyses of olivines in oceanic arc lavas by laser fluorination are significantly less variable than the whole-rock data (Eiler et al., 2000) and might highlight the role of subsolidus alteration on whole-rock samples. The progressive enrichment in whole-rock $\delta^{18}O$ in arc settings may reflect interaction of parental magmas with volcanic arc basement and continental crust. Notably, $\delta^{18}O$ values in the arc lavas from southeastern Guatemala correlate positively with SiO_2 so that the most evolved lavas have the highest $\delta^{18}O$ values (Fig. 7). Among the three different edifice types in southeastern Guatemala, BVF cinder cones exhibit the best correlation (r = 0.85) and fall closest to MORB in oxygen isotopic composition. The mean $\delta^{18}O$ of the BVF cinder cones (+6.8‰) still exceeds the average oxygen isotopic composition of continental arc basalts. VF stratovolcanoes display a relatively poor correlation (r = 0.41), and the subhorizontal trend roughly parallels the crystal fractionation trend (Fig. 7). Lava from VF stratovolcanoes have a mean $\delta^{18}O$ value of +7.0‰, whereas the OBVF central volcanoes have a higher mean at $\delta^{18}O$ = +7.2‰. A quartzite crustal sample has the highest $\delta^{18}O$ value measured in this study at 14.27‰. The granodiorite crustal sample has a $\delta^{18}O$ value of 3.71‰, suggesting alteration by a high temperature, meteoric fluid.

Light Element Contents

Boron (B) ranges from 1.1 to 22.9 ppm in the arc lavas from southeast Guatemala. The twenty-fold increase in abundance of

B underscores its highly incompatible chemical character. These analyses extend the narrow range of B concentration (2.4–15.2 ppm) found in an along-arc study of Central America (Leeman et al., 1994). The highest B values were recorded in more evolved lavas, and B contents correlate positively with SiO_2 (Fig. 8A).

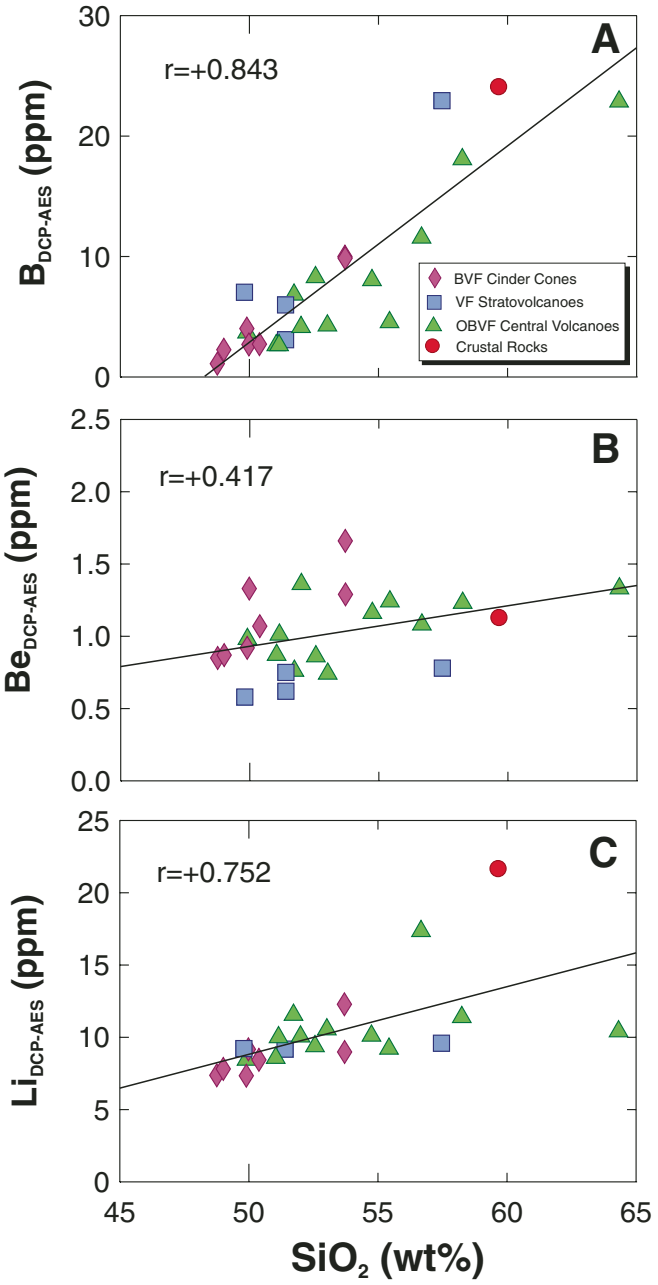

Figure 8. B, Be, and Li concentrations versus SiO_2. The positive correlations with SiO_2 reflect the incompatible nature of the light elements. (A) B. (B) Be. (C) Li. Only the granodiorite crustal sample is plotted to represent a possible contaminant because quartzite plots far off the SiO_2 scale. BVF—behind the volcanic front; OBVF—older behind the volcanic front; VF—volcanic front; DCP-AES—direct current plasma–atomic emission spectrometer.

VF stratovolcanoes and OBVF central volcanoes generally have higher B contents than the BVF cinder cones. Indeed, at a given SiO_2 content, VF stratovolcanoes tend to have slightly elevated B abundances relative to the central volcanoes and cinder cones. Granodiorite and quartzite samples taken to represent possible crustal contaminants contain B abundances comparable to the most enriched lavas (mean B of 23.1 ppm).

The 23 analyses reported here represent the first comprehensive study of Be in Guatemala. DCP-AES analyses of Be contents in rocks of this study display a limited range compared to B (0.6–1.7 ppm). The nearly threefold increase in Be affirms its less incompatible chemical character. Four other analyses record a limited range in Be of 0.5–0.8 ppm (Morris et al., 1990; Patino, 1997). In contrast to the behavior of B, the arc lavas exhibit a poor positive correlation between Be and SiO_2 and less systematic variation with respect to edifice type (Fig. 8B). Lavas from VF stratovolcanoes display the lowest Be contents, whereas BVF cinder cones and OBVF central volcanoes have a similar range of Be abundances and overall higher concentrations. At a given SiO_2 content, VF stratovolcanoes have lower Be abundances compared to the other edifice types. The two crustal samples analyzed cover a range of Be values (0.4–1.1 ppm) comparable to the lavas, with the granodiorite more enriched than the quartzite.

The Li analyses in this study represent the first compositional data of their type for arc lavas from Guatemala. Li contents analyzed by DCP-AES range between 7.3 and 17.3 ppm. The approximate twofold increase in Li concentrations suggests an incompatibility sequence of B >Be >Li. As for B and Be, a positive correlation exists between Li and SiO_2 (r = +0.75; Fig. 8C). BVF cinder cones generally have the lowest Li contents except for a sample far behind the volcanic front (GUC-25). VF stratovolcanoes exhibit uniform Li abundances of ~10 ppm and OBVF central volcanoes display the greatest variation from 8.4 to 17.3 ppm Li. The crustal samples span a larger range of Li composition than all the lavas with the granodiorite far exceeding the quartzite (21.7 versus 1.9 ppm Li).

DISCUSSION

Equilibrium in Minerals

Relations between bulk rock and phenocryst compositions provide a key perspective on whether a magma evolved in an open or closed system (Sakuyama, 1981; Hunter and Blake, 1995). Variations between mineral compositions and whole-rock compositions and assessment of whether equilibrium existed between mineral-mineral and mineral–whole-rock compositions lend insight into petrologic processes that influenced magma chemistry at depth. Obviously, these Guatemalan samples do not represent a cogenetic suite. The samples were collected from numerous locations at diverse edifice types. Indeed, the monogenetic nature of cinder cones essentially dictates sampling a single flow. Accordingly, this section places emphasis on the equilibrium approach. In fact, one might not expect systematic variation

in mineral chemistry with whole-rock compositions that do not represent a cogenetic suite. This caveat aside, the smooth major element trends suggest broadly common petrogenetic processes at Guatemalan volcanoes (Cameron et al., 2003).

Closed system evolution of a single magma chamber favors smooth systematic relationships between mineral and whole-rock chemistry (Davidson and de Silva, 1995; Hunter and Blake, 1995). However, the Guatemalan olivine phenocrysts show a range of compositions from Fo_{86} to Fo_{46} with no clear systematic variation with host rock composition (Figs. 3A and 3B). Groundmass olivine crystals exhibit similar compositional trends to the phenocryst rims (Fig. 3C). Compositional envelopes were drawn in Figure 3 to visually aid recognition of abrupt mineral chemical variations with changing whole-rock compositions. Mg numbers in clinopyroxene show an even more saw-toothed pattern of mineral variation with whole-rock composition (Fig. 4). A clinopyroxene phenocryst core from the most evolved sample analyzed records the maximum Mg number (Fig. 4A). Akin to clinopyroxene, Mg-rich orthopyroxene phenocrysts occur throughout the entire range of whole-rock compositions (Figs. 5A and 5B). Plagioclase phenocrysts exhibit many excursions to more anorthitic compositions at the basalt–basaltic andesite end of the whole-rock compositional spectrum but shift to a smooth declining trend at the andesite-dacite end (Figs. 6A and 6B). In summary, the overall lack of correlation between mineral chemistry and host lava composition hints strongly at the operation of open system processes. The existence of both normally and reversely zoned minerals in the same sample of some of the more evolved rocks suggests that magma mixing may be an important petrologic process. The lack of detailed compositional traverses across phenocryst phases prevents an extensive evaluation of this important petrologic process.

A more rigorous attempt to evaluate open system processes involves assessment of the degree of equilibrium attained by minerals with their host lavas. Under closed system fractional crystallization, equilibrium should exist between phenocryst cores and the whole-rock composition, between the groundmass melt and groundmass mineral phases, and between contiguous phenocrysts (Hunter and Blake, 1995). Consequently, plots of elemental ratios in minerals against identical ratios for bulk rocks should yield trends consistent with experimentally determined distribution coefficients.

Olivine-liquid $K_D^{Fe\text{-}Mg}$ values (where $K_D^{Fe\text{-}Mg}$ = $(FeO/MgO)_{olivine}/(FeO/MgO)_{whole\text{-}rock}$) decrease with increasing alkali content of coexisting liquid (Falloon et al., 1997). Based on the experiments of Falloon et al. (1997), a $K_D^{Fe\text{-}Mg}$ value of 0.32 would characterize a basaltic melt with an alkali content ($Na_2O + K_2O$) of ~5 wt%. This value falls in the intermediate range determined by a series of experiments run by Sisson and Grove (1993). Core compositions of olivine phenocrysts scatter well off the equilibrium line constructed using a $K_D^{Fe\text{-}Mg}$ of 0.32 (Fig. 9). A majority of the microprobe analyses plot above the equilibrium line in the field of olivine crystals too evolved for the whole-rock composition. Visual inspection of the data suggests that olivines from VF composite cones and OBVF central volcanoes stray further from the equilibrium line than olivine from BVF cinder cones.

An equilibrium $K_D^{Fe\text{-}Mg}$ value of 0.27 for orthopyroxene was determined by Gerlach and Grove (1982). In experimental melts, clinopyroxene has a slightly lower $K_D^{Fe\text{-}Mg}$ value of 0.23 (Grove and Bryan, 1983). Electron microprobe analyses of orthopyroxene phenocryst cores plot predominantly in the upper field of crystals too evolved for the whole-rock composition (Fig. 10A). The VF stratovolcano and OBVF central volcano orthopyroxene grains deviate equally from the equilibrium line into the upper field (Fig. 10A); no orthopyroxene phenocrysts were measured in the BVF cinder cones. At higher $FeO/MgO_{whole\text{-}rock}$ compositions, the orthopyroxene cores extend to higher $FeO/MgO_{orthopyroxene}$ contents. The core compositions of clinopyroxene phenocrysts plot in the upper evolved crystal field, although more data points fall below the equilibrium line than for orthopyroxene (Fig. 10B). Clinopyroxene cores from OBVF central volcanoes exhibit the largest deviations below the equilibrium line, whereas OBVF central volcano and VF stratovolcano clinopyroxene cores show equal departures above the equilibrium line over the entire range of $FeO/MgO_{whole\text{-}rock}$. One core analysis of a clinopyroxene microphenocryst from a BVF cinder cone lava plots far into the field for evolved crystals.

Melting experiments using basalts and basaltic andesites suggest that $K_D^{Ca\text{-}Na}$ values for plagioclase-melt equilibrium vary depending on the water content of the liquid (Sisson and Grove, 1993). Although independent of pressure, the $K_D^{Ca\text{-}Na}$ value increases from 1.1 under anhydrous conditions to 5.5 within H_2O-saturated magmas at 2 kbar (Sisson and Grove,

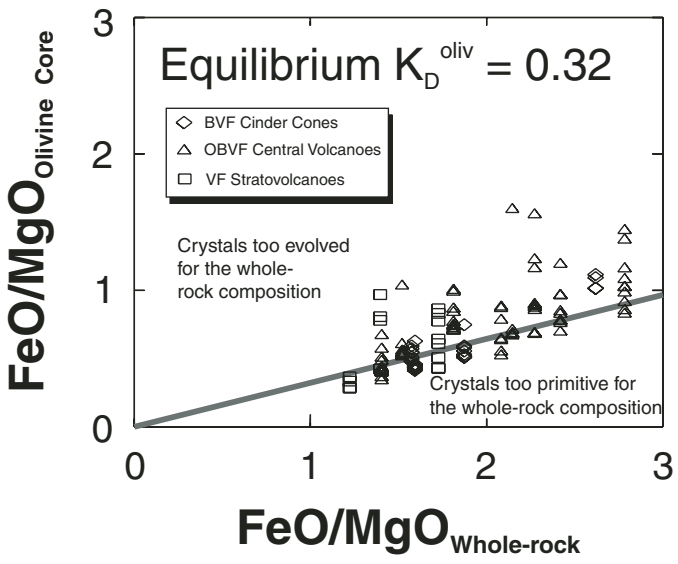

Figure 9. $FeO/MgO_{olivine}$ versus $FeO/MgO_{whole\text{-}rock}$. Core compositions of olivine phenocrysts largely fall above the equilibrium line (K_D = 0.32). BVF—behind the volcanic front; OBVF—older behind the volcanic front; VF—volcanic front.

1993). Variable compositions of the melt created by magmatic differentiation exert no control on the $K_D^{Ca\text{-}Na}$ value at constant water contents. Without an idea of the water content of the melt, interpreting the plagioclase equilibrium plot becomes a serious challenge. Water contents in melt inclusions hosted by olivines from both BVF cinder cones and VF stratovolcanoes are ~2.0 wt% (Walker et al., 2003). However, regardless of any reasonable water content and associated $K_D^{Ca\text{-}Na}$ value chosen, the plagioclase core compositional data exhibit disequilibrium. Isolated VF stratovolcano and OBVF central volcano samples plot well above the equilibrium lines in the primitive crystal field (Fig. 11). Plagioclase from BVF cinder cones show smaller deviations from the equilibrium lines, with more uniform intermediate compositions, suggestive of moderate water contents in agreement with the melt inclusion data.

In a very general sense, any mineral core that falls in the evolved crystal field almost certainly did not crystallize from a liquid similar in composition to the bulk rock. Instead, these minerals likely formed from a more evolved liquid. Geologic explanations for the mineral cores that are too primitive for the whole-rock composition include early-formed phases that failed to react with the surrounding melt or crystals inherited from a more primitive liquid during magma mixing. These latter types definitely constitute the minority in this study.

Owing to the lack of pyroxene phenocrysts in the BVF cinder cones and the uncertainty in melt water contents with respect to plagioclase, we use olivine compositional data to try to determine whether closed or open system behavior was taking place. An argument for closed system behavior can be made if the electron microprobe did not analyze true olivine cores, but instead zones rimward of these points. True cores would be strictly defined as the first solid crystallizing from the bulk liquid. Thin sections are two-dimensional slices through a three-dimensional crystal, so there is no guarantee that the true core is analyzed when the electron beam is positioned at the center of a phenocryst. Thus, the numerous analyses that plot above the equilibrium line in the evolved field represent parts of the mineral that crystallized from interstitial liquid slightly more evolved than the bulk rock composition but still under equilibrium conditions. Although there is a coherent positive correlation between minimum FeO/MgO olivine core compositions with whole-rock FeO/MgO, the lack of true core compositions relative to rims plotting on the equilibrium line is troublesome.

If deviations from the mineral equilibrium line do indeed reflect disequilibrium and open system processes in the magma chamber, then the magnitude of the deviation logically holds important information on the extent of the process. It becomes a trivial matter to calculate the mean deviation from the olivine equilibrium line for each volcano type. Olivine cores from BVF cinder cones have a range in deviations from the equilibrium line of −0.12 to +0.29 with a mean of 0.01. OBVF central volcanoes have a range of deviations from −0.14 to +0.90 with a mean of 0.10, and VF stratovolcanoes exhibit a range of −0.11 to +0.56 with a mean deviation of 0.12. Based on the magnitudes of these deviations, the open system process seems more prevalent at the VF stratovolcanoes and OBVF central volcanoes.

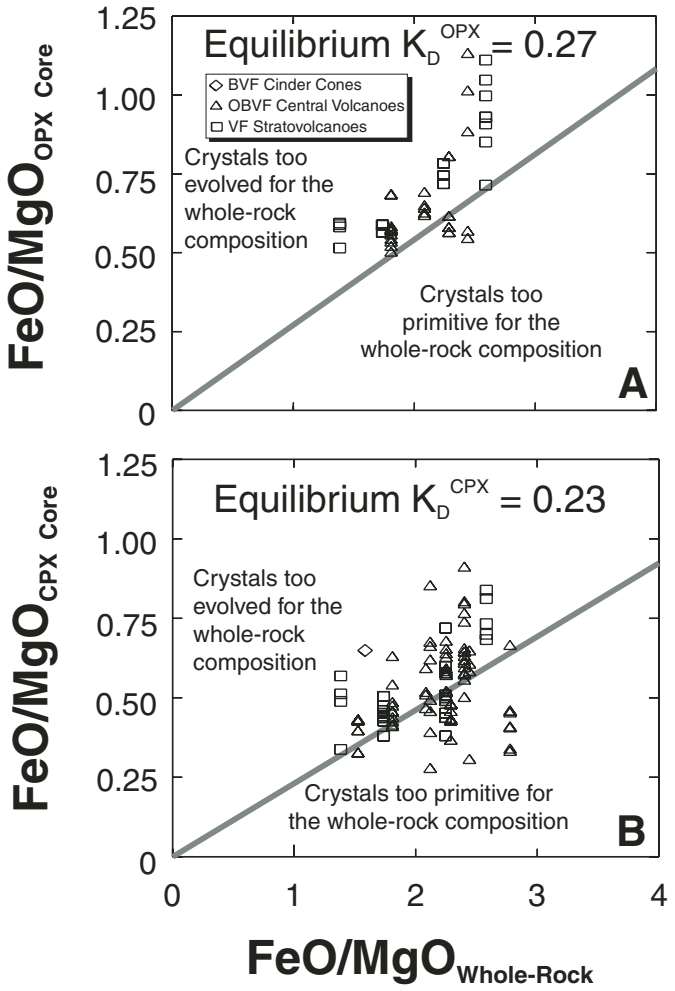

Figure 10. $FeO/MgO_{pyroxene}$ versus $FeO/MgO_{whole\text{-}rock}$ diagrams. (A) Orthopyroxene (OPX) phenocryst core data plot largely above an equilibrium defined by $K_D = 0.27$. (B) Clinopyroxene (CPX) phenocryst core data also plot largely above the equilibrium line defined by $K_D = 0.23$. BVF—behind the volcanic front; OBVF—older behind the volcanic front; VF—volcanic front.

Assuming that true core regions of phenocrysts were analyzed more often than not by the electron microprobe, the nonsystematic variation of mineral chemistry with whole-rock composition and the nonequilibrium mineral core compositions together lead to the conclusion that open system processes played a significant role in creating compositional diversity in the Guatemalan lavas.

Oxygen Isotope Variations

Two features of the whole-rock $\delta^{18}O$ data warrant comment. First, the arc lavas of southeastern Guatemala have elevated values of $\delta^{18}O$ compared to their respective global counterparts. The

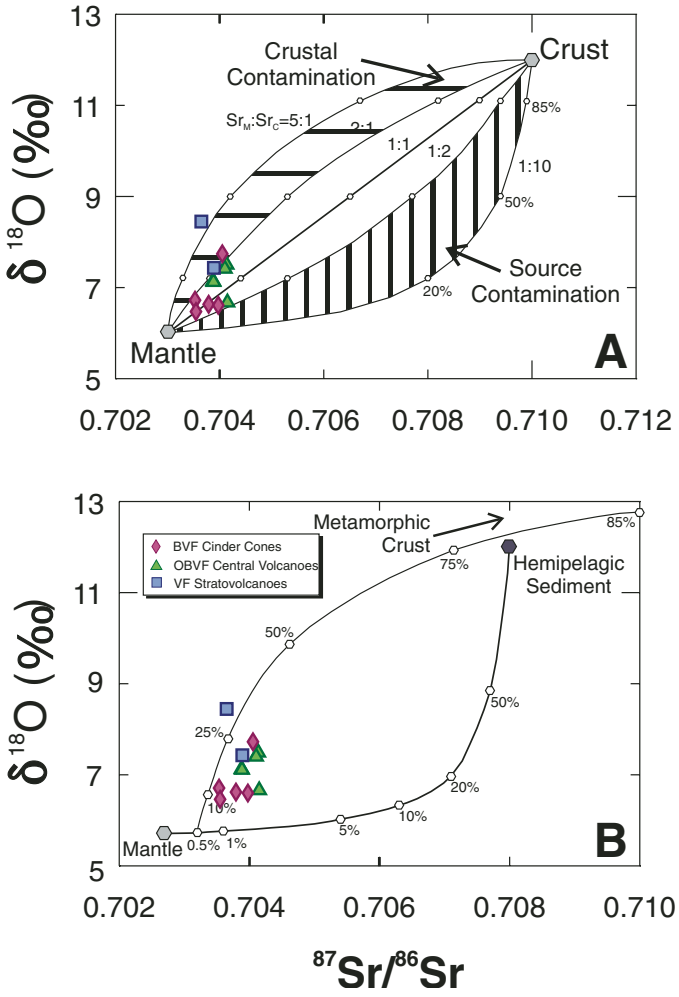

Figure 11. CaO/Na$_2$O$_{plagioclase}$ versus CaO/Na$_2$O$_{whole\text{-}rock}$ diagram. The equilibrium K_D value depends on the water content of the magma. K_D values of 1.1, 3.4, and 5.5 are shown. The scatter exhibited by the plagioclase core data suggests disequilibrium behavior. BVF—behind the volcanic front; OBVF—older behind the volcanic front; VF—volcanic front.

range in BVF cinder cones from 6.16 to 7.74‰ falls above the global mean for whole-rock backarc basins of 6.0‰ (Harmon and Hoefs, 1995). Likewise, the range for VF stratovolcanoes of 6.36–8.46‰ lies above the mean for continental arc basalts of 6.2‰ (Harmon and Hoefs, 1995). Second, relatively large ranges in $\delta^{18}O$ characterize the basalts and evolved lavas from southeastern Guatemala.

Crystal Fractionation

The positive correlation between $\delta^{18}O$ and SiO_2 might suggest that crystal fractionation played an important role in the chemical variation (Fig. 7). However, the small isotopic fractionations that occur between melt and crystals at high temperature suggest that crystal differentiation has little influence in changing the $\delta^{18}O$ of evolving magmas. Oxygen isotope studies of closed system magmatic suites confirm this general observation (Muehlenbachs and Byerly, 1982; Chivas et al., 1982; Kalamarides, 1984). At the Galapagos Spreading Center, 90% fractionation from low K-tholeiite to rhyodacite only enriched the residual melt by ~1.2‰ (Muehlenbachs and Byerly, 1982). Crystal fractionation in the Koloula Igneous Complex on the island of Guadalcanal generated $\delta^{18}O$ values that range from 5.7 to 7.2‰ (Chivas et al., 1982). $\delta^{18}O$ values of the Kiglapait layered intrusion vary from 6.0‰ for the first liquids in the Lower Zone to 6.3‰ for the final liquids in the Upper Zone (Kalamarides, 1984). Thus, empirical knowledge suggests that the range of $\delta^{18}O$ values in the Guatemalan arc lavas exceeds the normal fractionation spread. In fractionating suites of magmas with demonstrable closed system behavior, the slope of the $\delta^{18}O$ versus SiO_2 diagram varies according to temperature.

Further insight on the $\delta^{18}O$ variations can be gleaned from quantitative modeling (Sheppard and Harris, 1985; Grunder, 1987; Woodhead et al., 1987; Harmon and Gerbe, 1992; Singer et al., 1992). Closed system Raleigh fractional crystallization enriches the residual liquid in $\delta^{18}O$ according to the equation:

$$\delta^{18}O_{melt}{}^{t} = (\delta^{18}O_{melt}{}^{i} + 1000)\, f^{(\alpha - 1)} - 1000, \quad (1)$$

where $\delta^{18}O_{melt}{}^{t}$ is the $^{18}O/^{16}O$ ratio of the magma after some finite amount of crystal fractionation, $\delta^{18}O_{melt}{}^{i}$ is the initial $^{18}O/^{16}O$ ratio of the magma prior to fractionation processes, f is the fraction of melt remaining at time t, and α is the mean crystal-melt fractionation factor. In high temperature magmatic systems, α values approximate unity, so the relative enrichment of the crystal-melt phases in ^{18}O is given simply by

$$\Delta_{A-B}\,(‰) = 10^3 \ln \alpha_{A-B} = \delta_A - \delta_B. \quad (2)$$

The mean fractionation factor can be uniquely calculated for distinct stages in the evolutionary history of the Guatemalan magmas. The calculation involves multiplying the molar proportion of each phase by the mole fraction of oxygen in each phase and the mean $\delta^{18}O$ fractionations between crystal and melts taken from the literature (e.g., Sheppard and Harris, 1985; Kalamarides, 1986). Substitution of the mean fractionation factor into the general Raleigh fractionation formula allows calculation of the expected $\delta^{18}O$ value of residual melts.

Table 5 provides the details of least squares crystal fractionation model developed to support interpretation of the oxygen isotope data. In Stage 1, 28.6% crystallization of plagioclase, clinopyroxene, and olivine from parent magma GUC-800 (recalculated SiO_2 = 49.53%) yields the daughter magma GCH-01 (recalculated SiO_2 = 52.04%) with an acceptable r^2 = 0.805. The mean fractionation factor ($\Delta_{xl\text{-}melt}$) is –0.06 or α = 0.99994. The calculated $\delta^{18}O_{melt}$ after 28.6% crystallization using a $\delta^{18}O_{melt}{}^{i}$ of 6.21‰ is 6.23‰.

Plagioclase, clinopyroxene, olivine, and titanomagnetite could crystallize from GCH-01 in Stage 2 to produce a nearly equal volume of daughter melt similar in composition to FEL-3 (recalculated SiO_2 = 60.83%) with r^2 = 0.880. The resulting $\Delta_{xl\text{-}}$

TABLE 5. LEAST SQUARES MIXING CRYSTAL FRACTIONATION MODEL

Stage	Parent	Proportion	Percentage	Mineral	Fit
1	GUC-800	0.123	43.30%	Plagioclase (An_{92})	r^2 = 0.805
		0.12	42.30%	Cpx (Wo_{46}-En_{37}-Fs_{17})	
		0.041	14.30%	Olivine (Fo_{72})	
		0.714		GCH-01 (daughter)	
2	GCH-01	0.029	6.00%	Ti-magnetite (Ti_{10})	r^2 = 0.880
		0.263	56.00%	Plagioclase (An_{67})	
		0.085	18.00%	Cpx (Wo_{44}-En_{47}-Fs_{9})	
		0.093	19.80%	Olivine (Fo_{68})	
		0.517		FEL-3 (daughter)	
3	FEL-3	0.04	11.00%	Ti-magnetite (Ti_{12})	r^2 = 0.095
		0.256	71.00%	Plagioclase (An_{59})	
		0.023	6.30%	Cpx (Wo_{42}-En_{44}-Fs_{14})	
		0.042	11.70%	Olivine (Fo_{60})	
		0.638		GAG-13A (daughter)	

$_{melt}$ is –0.121 or α = 0.99988. The Raleigh fractionation formula yields a calculated $\delta^{18}O$ of 6.31‰ for the melt.

In Stage 3, 46.2% crystallization of plagioclase, clinopyroxene, olivine, and titanomagnetite from a FEL-3 parental melt produces a daughter magma GAG-13A (recalculated SiO_2 = 69.81%) with a very low r^2 of 0.095. More significant titanomagnetite fractionation increased the mean fractionation factor (Δ) to –0.492 or α = 0.99951. The calculated $\delta^{18}O_{melt}$ ^{t} at the end of the fractionating sequence is 6.53‰. Large shifts in $\delta^{18}O$ of magma (i.e., >1‰) result only through the removal of significant amounts of either an ^{18}O-depleted phase such as olivine or an oxide mineral or an ^{18}O-enriched phase such as quartz (Harmon and Gerbe, 1992). Otherwise, closed system differentiation of magma from a basalt to rhyolite generates much smaller variations in $\delta^{18}O$. The predominance of plagioclase in the fractionating assemblage of calc-alkaline magmatic systems often results in $\delta^{18}O$ changes of <0.5. Table 6 presents a summary of the calculated variations in $\delta^{18}O$ of a melt dictated by crystal fractionation only. The oxygen isotope variations traced through the three stages define a near-horizontal crystal fractionation line on the $\delta^{18}O$ versus SiO_2 diagram (Fig. 7). Open-system processes produce deviant $\delta^{18}O$-SiO_2 arrays compared with the near-horizontal crystal fractionation trend when the contaminant has an isotopic signature distinct from the melt (Harmon and Gerbe, 1992). Mafic to intermediate magmas that assimilate ^{18}O-rich crust during differentiation form steep, positive $\delta^{18}O$-SiO_2 trends (Davidson and Harmon, 1989; Ellam and Harmon, 1990), whereas assimilation of ^{18}O-depleted crustal rocks modified by meteoric hydrothermal alteration yield negative $\delta^{18}O$-SiO_2 arrays (Grunder, 1987; Harmon and Gerbe, 1992). The positive array with a Spearman rank correlation coefficient of +0.738 defined by the Guatemalan arc lavas (Fig. 7) favors involvement of an enriched ^{18}O contaminant. The groundmass of lava flows readily exchange oxygen during low temperature weathering or interaction with hydrothermal fluids, and conceivably could account for some of the positive shift in the $\delta^{18}O$ data. The random nature of alteration argues against it being a significant variable in light of the respectable correlation between $\delta^{18}O$ and SiO_2. Trace element mobility has been documented in spheroidally weathered Guatemalan lavas (Patino et al., 2003), but this study avoided visibly weathered samples and collected only the freshest samples from the volcanoes in question. Ideally, complementary measurements of the oxygen isotopic composition of refractory minerals such as olivine or clinopyroxene by laser fluorination or ion microprobe techniques would more accurately determine magmatic values (Singer et al., 1992; Macpherson and Mattey, 1998; Eiler et al., 1998, 2000; Dorendorf et al., 2000; Vroon et al., 2001). Correction procedures based on assumptions of primary H_2O contents generally result in small adjustments of $\delta^{18}O$ values. Lavas from Martinique in the Lesser Antilles typically had measured $\delta^{18}O$ reduced by <0.5‰ (Davidson and Harmon, 1989). Owing to the young age and fresh nature of the Guatemalan lavas in thin section and the small modifications attributed to water uptake, crustal contamination plays a more prominent role in enriching the magmas in $\delta^{18}O$.

TABLE 6. CALCULATED VARIATIONS IN $\delta^{18}O$ OF A MELT CONTROLLED BYCRYSTAL FRACTIONATION

Model	$\delta^{18}O$ Values		Mean Δ (‰)	$\Delta = \delta^{18}O_{xl} - \delta^{18}O_{magma}$			
	Parent	Daughter		Plag	Cpx	Oliv	Mt
Stage 1	6.21	6.23	–0.06	0.2	–0.2	–0.5	0
Stage 2	6.23	6.31	–0.121	0.2	–0.2	–0.5	–1.9
Stage 3	6.31	6.53	–0.492	0	–1	–1.8	–3.6

Source versus Crustal Contamination

Oxygen isotopic compositions in combination with radiogenic isotopes can distinguish, in principle, between crustal and source contamination (James, 1981). Sr/O ratios of the mantle and crustal end members define mixing trajectories on a plot of $\delta^{18}O$ versus $^{87}Sr/^{86}Sr$ (Fig. 12). The high Sr content of mafic magmas compared to that of the potential crustal contaminants accounts for a convex crustal contamination mixing curve.

Conversely, the low Sr content of the bulk mantle relative to subducted crustal material accounts for a concave source contamination trend. Partial melting of mantle peridotite produces primary magma enriched in incompatible elements such as Sr and Nd relative to lithologies of the continental crust. In sharp contrast, the bulk mantle has low incompatible element contents relative to enriched sediments and thus represents the depleted end member in the source contamination case. These differing chemical characteristics produce convex trajectories for crustally contaminated arc magmas and concave trends after recycling sediments into a MORB-like subarc mantle source.

Whole-rock oxygen isotopic data have poor but positive correlations with the Sr isotopic composition of the Guatemalan arc lavas. Mixing curves can be calculated using the binary mixing equation:

$$R^X_M = [R^X_A X_A f + R^X_B X_B (1 - f)]/[X_A f + X_B (1 - f)], \quad (3)$$

where R^X_M is the isotope ratio of Sr or O in a mixture of components A and B, X_A and X_B are concentrations of Sr or O in A and B, and f is the weight fraction of A. Each curve was calculated using a different ratio of Sr in the mantle versus Sr in the crust (i.e., Sr_M:Sr_C). Five different concentrations (100, 40, 20, 10, and 2 ppm) were assumed for the mantle, whereas the enriched end member was taken to have a Sr concentration of 20 ppm. The model calculations assume equal concentrations of O in the two end members but different $\delta^{18}O$ values of 6.0‰ for the mantle and 12.0‰ for the crust. Varying values of f and substitution of these concentrations into the general two-component binary mixing equation generates the five separate curves. The data plot within or in close proximity to the field representing magmas contaminated by continental crust (Fig. 12A). The spread of the data suggests that between 5% and 35% crustal material is added to the parental arc magma.

A more detailed, two-stage model can be constructed based on the distribution of data in the simple model using more geochemically relevant parameters. Two-stage models have been successful in explaining Sr and O isotopic relationships in the Marianas (Woodhead et al., 1987) and the Aeolian Islands (Ellam and Harmon, 1990). Source contamination shifts the data away from the mantle source in the direction of higher $^{87}Sr/^{86}Sr$, whereas crustal contamination profoundly increases the $\delta^{18}O$ contents of the magma compared to only moderate increases in $^{87}Sr/^{86}Sr$. Again, oxygen concentrations were assumed to be constant in all components. The mantle Sr concentration of 15 ppm (Chen and Frey, 1985), $^{87}Sr/^{86}Sr$ ratio of 0.7027 (Zindler and Hart, 1986), and $\delta^{18}O$ of 5.7 (Woodhead et al., 1987) characterize a MORB source. The mean hemipelagic sediment from Deep Sea Drilling Project (DSDP) Site 495 off Guatemala has ~300 ppm Sr and a $^{87}Sr/^{86}Sr$ ratio of 0.708 (Patino, 1997). The sediments from DSDP 495 were not analyzed for $\delta^{18}O$. Unaltered hemipelagic sediment from Middle Valley in the northern Pacific Ocean has $\delta^{18}O$ values that approach 12.0‰ (Goodfellow et al., 1993). Extrapolation of the Guatemalan Sr-SiO_2 trend back to a SiO_2 content of 46% approximates the composition of a hypothetical primitive arc magma in Guatemala and yields the model Sr abundance for the magma of 750 ppm. The magma $^{87}Sr/^{86}Sr$ ratio of 0.7032 and $\delta^{18}O$ value of 5.73 were products of the Stage 1 model calculation of 0.5% sediment contamination in the source. Finally, quartzite in southeastern Guatemala has Sr contents of ~30 ppm, a $^{87}Sr/^{86}Sr$ ratio of 0.740, and a $\delta^{18}O$ value of 14.0‰ (Walker et al., 1995; this study). The quartzite sample was incorporated into the model simply because of the altered nature and unrealistically low $\delta^{18}O$ value of 3.71‰ determined for the granodiorite sample. The high $\delta^{18}O$ value of the quartzite used in this model would approximate other more likely crustal contaminants.

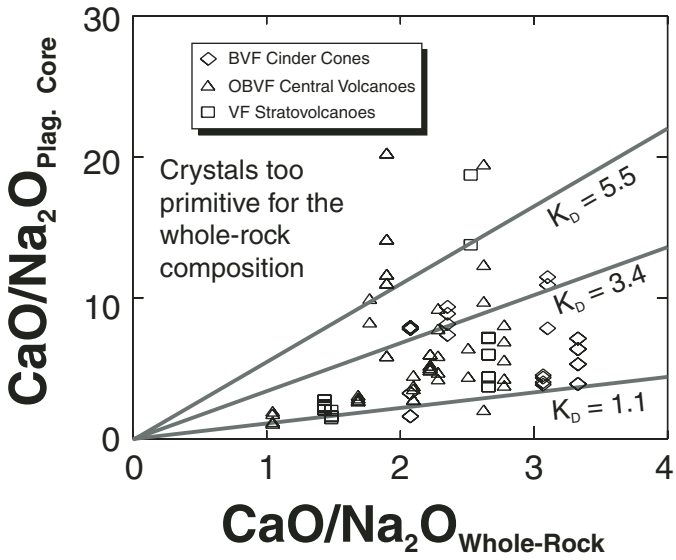

Figure 12. (A) $\delta^{18}O$ versus $^{87}Sr/^{86}Sr$ diagram (James, 1981). The Guatemalan arc lavas plot within the field of magmas contaminated by continental crust as opposed to mantle contaminated by sediments. (B) Diagram of $\delta^{18}O$ versus $^{87}Sr/^{86}Sr$ showing a two-stage evolution model for arc lavas from southeastern Guatemala. Crustal contamination of primary magmas by metamorphic crustal samples follows limited contamination of the mantle by hemipelagic sediments. A series of mixing hyperbolas between sediment-modified mantle and crustal contaminants would best fit the spread of data points. BVF—behind the volcanic front; OBVF—older behind the volcanic front; VF—volcanic front.

The two-stage model illustrated in Figure 12B represents a more realistic explanation of the contamination history in Guatemala. A combination of between 0.5% and 2.0% hemipelagic sediment addition to a MORB-source mantle and subsequent mixing of magma with between 10% and 30% metamorphic crustal material could explain the Sr-O isotopic data. The proposed two-stage process conforms to the general conceptual model for arc magmatism in which material transfer at the slab-mantle wedge interface induces partial melting and ascending magmas digest crustal materials during stagnation in reservoirs at various depths.

Effects of Crustal Contamination on Elemental Concentrations

Plots of various elements versus $\delta^{18}O$ should convey information about elemental inputs to magmas during crustal contamination assuming that assimilation accounts for increases in $\delta^{18}O$. Two statistical quantities contribute valuable insight into the nature of the relationship between the two participating variables. The Spearman rank correlation coefficient *r* essentially measures how well the data fit a straight line. A high value of *r* represents a high degree of correlation. The threshold *r* value that indicates a statistically significant correlation depends on the number of samples. On the other hand, the slope of the linear regression line relates to the dependence or independence of one variable relative to the other. Simple examples illustrate their interpretative value. A data set with a high *r* value near one and a slope near zero suggests an excellent correlation, but also that *y* is independent of *x*. A second data set with $r = 0.75$ and $m = 1$ indicates a moderate to good correlation and that *y* depends on *x*, or in geochemical phrasing, *y* and *x* behave similarly. In the current discussion, $\delta^{18}O$ is used to evaluate the effect of crustal contamination on critical incompatible elements. Spearman rank correlation coefficients screen combinations for statistical significance, whereas slope measures the magnitude of the behavioral similarity.

Overall, incompatible element versus $\delta^{18}O$ plots feature relatively high Spearman rank correlation coefficients. The key threshold value for correlation coefficients with a 0.1% level of significance are 0.618 at $n = 23$ (LeMaitre, 1982). Be, Sb, and La have correlation coefficients below the threshold value and consequently appear unrelated to $\delta^{18}O$. Compilation of the slope data suggests that incompatible elements exhibit a complete spectrum of coherency with $\delta^{18}O$ directly and crustal contamination indirectly (Fig. 13). Crustal contamination more significantly affects those incompatible elements with a slope of ~1 or greater (i.e., B, La, Pb, Li, and Th). Assimilation of crust exerts less control on incompatible element concentrations of Rb, Sb, Ba, and Be based on slopes <0.3. An intermediate group of elements with slopes between 0.3 and 0.9 consists of Cs and U. Thus, the sequential order of the incompatible elements on the *x*-axis from left to right in Figure 13 serves as a relative measure of the chemical influence of crustal contamination.

Igneous petrologists rely heavily on incompatible trace element ratios to provide important petrogenetic information. Common differentiation processes such as crystal fractionation and partial melting have little effect on ratios involving trace elements with similar degrees of incompatibility. Thus, any information on the nature of elemental modification by crustal contamination helps petrologists make more intelligent decisions when assembling these key trace element ratios. Crustal contamination will influence a ratio formed from elements with disparate slopes (Fig. 13). B/Be ratios in Guatemalan arc lavas correlate positively with SiO_2 and trend toward but do not exceed the field of crustal rocks (Fig. 14A). Many studies of continental arc lavas indiscriminately use B/Be as a measure of the slab signature

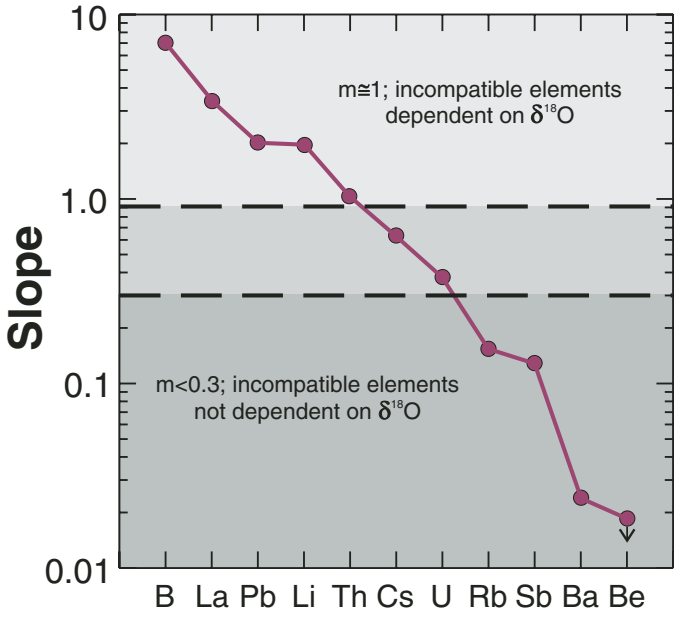

Figure 13. Magnitude of the slope for select trace elements and $\delta^{18}O$. Given that slope measures the interdependency of variables on variation diagrams, elements with slopes greater than 0.9 have been most affected by crustal contamination.

without thorough assessment of the control exercised by crustal contamination. The effects of crustal contamination will be canceled out in ratios involving elements with similar slopes. Not only does a poor correlation exist between Ba/La versus SiO_2, but many of the lavas possess higher Ba/La ratios than the analyzed crustal rocks (Fig. 14B). Accordingly, Ba/La monitors slab signatures much better than a ratio such as B/Be in an arc with thick continental crust.

Edifice Style and Crustal Contamination

Porphyritic lavas with low-pressure phase assemblages develop at the large stratovolcanoes of the VF owing to extensive crystallization in shallow magma chambers. Analogous rocks with similar phenocryst assemblages occur at OBVF central volcanoes. In sharp contrast, the mafic BVF cinder cone lavas have aphyric textures and were produced by small volume eruptions associated with the extensional regime of the Ipala Graben. These diffuse vents often coincide with systematic lineaments interpreted as deep crustal structures. The whole-rock oxygen isotope data support this volcanological scenario. The highly elevated $\delta^{18}O$ values measured at the VF stratovolcanoes and OBVF central volcanoes result from crustal assimilation accompanying fractional crystallization in high-level magma chambers. Erupted lavas have common low-pressure phenocryst phases and evolved whole-rock compositions altered by the assimilation of crustal contaminants. The slightly elevated $\delta^{18}O$ values observed in the BVF cinder cone lavas indicate that the magmas ascended

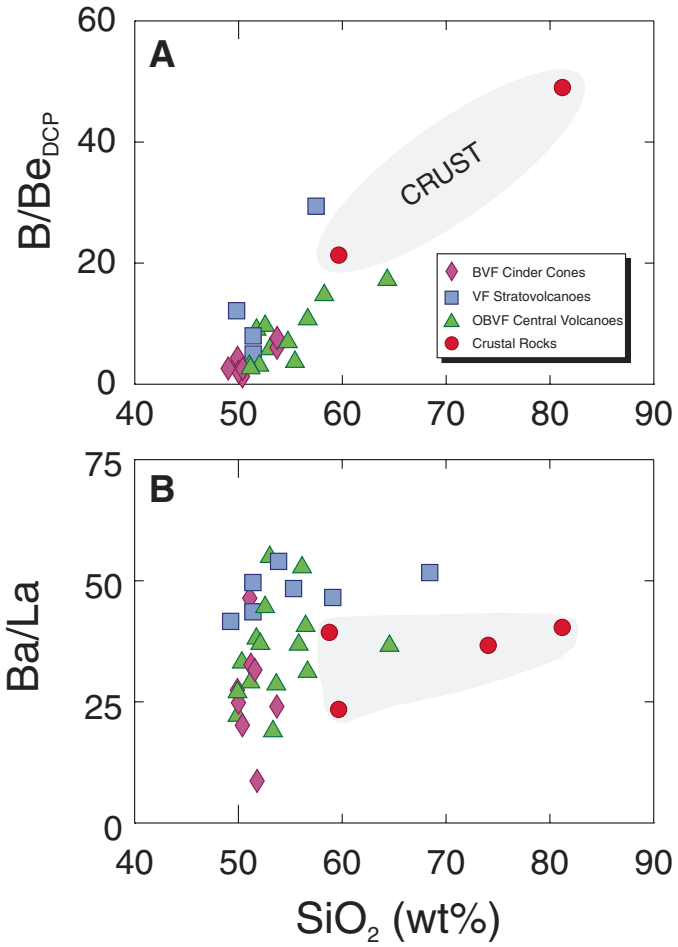

Figure 14. Critical trace element ratios versus SiO_2. (A) B/Be versus SiO_2. Guatemalan arc lavas essentially plot on a mixing line between mantle and crust. (B) Ba/La versus SiO_2. Ba/La in Guatemalan arc lavas exceeds that recorded in possible crustal contaminants. Ba/La ratio was less affected by crustal contamination than B/Be. BVF—behind the volcanic front; OBVF—older behind the volcanic front; VF—volcanic front; DCP—direct current plasma.

more rapidly from deep crustal magma chambers underlying the extended crust. These eruptive products have more mafic compositions, an aphyric to sparsely olivine-phyric texture, and little chemical crustal signature. Short residence times in shallow reservoirs suggest that the small enrichment in $\delta^{18}O$ probably records deeper crustal contamination processes. Unusual trends on Pb isotope plots for the BVF cinder cones identified granulitic crust as a possible contaminant (Walker et al., 1995). Curiously, cinder cone lavas in Mexico seemed vulnerable to crustal assimilation based on their B/Be-SiO_2 relationships (Hochstaedter et al., 1996). Small batches of magma from monogenetic centers in Mexico traversed separate sections of crust, and therefore may be more susceptible to crustal contamination. A supplementary oxygen isotope study in the Mexican volcanic belt might help resolve this discrepancy.

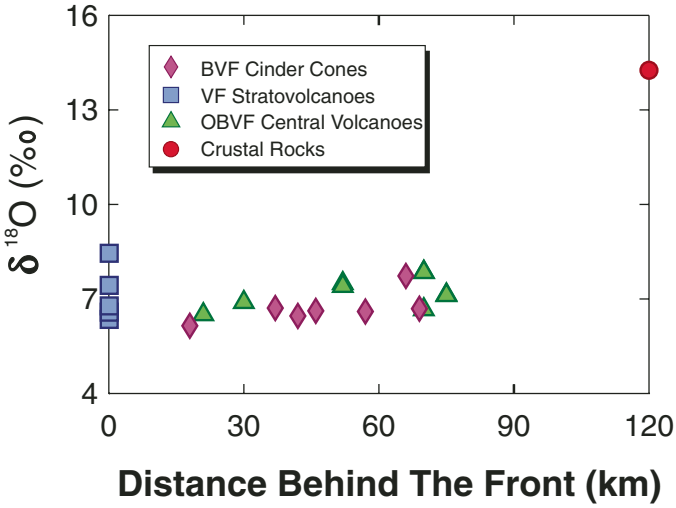

Figure 15. $\delta^{18}O$ versus distance behind the volcanic front in southeastern Guatemala. $\delta^{18}O$ remains essentially constant at behind the volcanic front (BVF) cinder cones across the arc, implying no absolute increase in crustal contamination. BVF cinder cones have $\delta^{18}O$ values only slightly above normal mid-oceanic ridge basalt. OBVF—older behind the volcanic front; VF—volcanic front.

Across-Arc Changes in $\delta^{18}O$

Nd and Pb isotopic ratios in BVF cinder cones display relatively consistent and continuous across-arc changes: both $^{207}Pb/^{204}Pb$ and $^{208}Pb/^{204}Pb$ generally increase, whereas $^{143}Nd/^{144}Nd$ declines with distance behind the front (Walker et al., 1995). Either an absolute or apparent increase in crustal contamination across the arc can explain the regular radiogenic isotopic variations. Walker et al. (1995) discounted an absolute increase in the amount of contamination as unreasonable owing to the likelihood of rapid magma ascent caused by tectonic extension behind the front. Instead, assimilation of older, more isotopically evolved crust farther behind the front only creates the illusion of increasing extents of crustal contamination. Oxygen-isotopic compositions do not evolve with age like the radiogenic isotopes, and therefore offer another means of evaluating this question. The $\delta^{18}O$ values of the BVF cinder cones remain relatively constant across the arc (Fig. 15), ruling out the possibility that the overall amount of contamination increases behind the front. The highest $\delta^{18}O$ values occur at VF stratovolcanoes and at OBVF central volcanoes.

CONCLUSIONS

Geochemical studies of Guatemalan arc lavas demonstrate the importance of open system processes in modifying mantle melts. Mineral chemistry varies nonsystematically with whole-rock compositions and together with disequilibrium core compositions in olivine, pyroxene, and plagioclase indicate that the

crustal magma chambers behave as an open system. Whole-rock oxygen isotope data are compatible with crustal contamination being an important open system process in southeastern Guatemala. Crystal fractionation cannot explain the large ranges in $\delta^{18}O$ measured in the erupted lavas. Rather, steep arrays on the $\delta^{18}O$-SiO_2 diagram favor incorporation of ^{18}O-rich crustal rocks during ascent of primitive magmas. Enrichments in $\delta^{18}O$ imposed by low-temperature weathering or alteration likely prove insignificant compared to the effects of crustal contamination. Combined Sr and O isotope models indicate minor additions of 0.5%–1% sediment to the mantle wedge followed by variable degrees of crustal contamination between 10% and 30%. Lower $\delta^{18}O$ values from BVF cinder cones compared to the stratovolcanoes of the VF and OBVF suggest that relatively lower amounts of crustal contamination accompany smaller scale, deeper magmatic systems. Extension associated with the Ipala Graben promoted short crustal residence times for the mafic cinder cone magmas and contributed to the lower $\delta^{18}O$ values. Variations in $\delta^{18}O$ better reflect the magnitude of the crustal contamination process than the age-controlled radiogenic isotopes. Open system processes such as crustal contamination and magma mixing might control eruption style, leading to the construction of different edifice types. More significant volcanic hazards would therefore be associated with the eruption of VF stratovolcanoes and OBVF central volcanoes.

ACKNOWLEDGMENTS

The authors wish to thank Ian Richards for help collecting the oxygen isotopic data at Southern Methodist University. Jeff Ryan provided access to his direct current plasma laboratory at University of South Florida for the light element chemistry. Ian Steele assisted with the mineral chemical data at the University of Chicago. Mark Feigenson at Rutgers opened his lab to collect the Sr isotopic data. Detailed and constructive reviews by Richard Conrey, Todd Feeley, and Gregg Bluth were extremely helpful in improving the manuscript.

REFERENCES CITED

Cameron, B.I., Walker, J.A., Carr, M.J., Patino, L.C., Matías, O., and Feigenson, M.D., 2003, Flux versus decompression melting at stratovolcanoes in southeastern Guatemala: Journal of Volcanology and Geothermal Research, v. 119, p. 21–50, doi: 10.1016/S0377-0273(02)00304-9.

Carr, M.J., 1984, Symmetrical and segmented variation of physical and geochemical characteristics of the Central American volcanic front: Journal of Volcanology and Geothermal Research, v. 20, p. 231–252, doi: 10.1016/0377-0273(84)90041-6.

Carr, M.J., Feigenson, M.D., and Bennett, E.A., 1990, Incompatible element and isotopic evidence for tectonic control of source mixing and melt extraction along the Central American arc: Contribution to Mineralogy and Petrology, v. 105, p. 369–380, doi: 10.1007/BF00286825.

Chen, C.Y., and Frey, F.A., 1985, Trace element and isotopic geochemistry of lavas from Haleakala volcano, east Maui, Hawaii: Implications for the origin of Hawaiian basalts: Journal of Geophysical Research, v. 90, p. 8743–8768.

Chivas, A.R., Andrew, A.S., Sinha, A.K., and O'Neil, J.R., 1982, Geochemistry of a Pliocene-Pleistocene oceanic-arc plutonic complex, Guadalcanal: Nature, v. 300, p. 139–143, doi: 10.1038/300139a0.

Davidson, J.P., and Harmon, R.S., 1989, Oxygen isotope constraints on the petrogenesis of volcanic arc magmas from Martinique, Lesser Antilles: Earth and Planetary Science Letters, v. 95, p. 255–270, doi: 10.1016/0012-821X(89)90101-5.

Davidson, J.P., and de Silva, S., 1995, Late Cenozoic magmatism of the Bolivian Altiplano: Contributions to Mineralogy and Petrology, v. 119, p. 387–408.

Davidson, J.P., McMillan, N.J., Moorbath, S., Worner, G., Harmon, R.S., and Lopez-Escobar, L., 1990, The Nevados de Pachachata volcanic region (18 S/69 W, N. Chile) II. Evidence for widespread crustal involvement in Andean magmatism: Contributions to Mineralogy and Petrology, v. 105, p. 412–432, doi: 10.1007/BF00286829.

Dorendorf, F., Wiechert, U., and Wörner, G., 2000, Hydrated sub-arc mantle: a source for the Kluchevskoy volcano, Kamchatka/Russia: Earth and Planetary Science Letters, v. 175, p. 69–86, doi: 10.1016/S0012-821X(99)00288-5.

Eiler, J.M., McInnes, B., Valley, J.W., Graham, C.M., and Stolper, E.M., 1998, Oxygen isotope evidence for slab-derived fluids in the sub-arc mantle: Nature, v. 393, p. 777–781, doi: 10.1038/31679.

Eiler, J.M., Crawford, A., Elliot, T., Farley, K.A., Valley, J.W., and Stolper, E.M., 2000, Oxygen isotope geochemistry of oceanic-arc lavas: Journal of Petrology, v. 41, p. 229–256, doi: 10.1093/petrology/41.2.229.

Ellam, R.M., and Harmon, R.S., 1990, Oxygen isotope constraints on the crustal contribution to the subduction-related magmatism of the Aeolian Islands, southern Italy: Journal of Volcanology and Geothermal Research, v. 44, p. 105–122, doi: 10.1016/0377-0273(90)90014-7.

Falloon, T.J., Green, D.H., O'Neill, H., St, C., and Hibberson, W.O., 1997, Experimental tests of low degree peridotite partial melt compositions: Implications for the nature of anhydrous near-solidus peridotite melts at 1 GPa: Earth and Planetary Science Letters, v. 152, p. 149–162, doi: 10.1016/S0012-821X(97)00155-6.

Feeley, T.C., and Sharp, Z.D., 1995, $^{18}O/^{16}O$ isotope geochemistry of silicic lava flows erupted from Volcan Ollague, Andean Central Volcanic Zone: Earth and Planetary Science Letters, v. 133, p. 239–254, doi: 10.1016/0012-821X(95)00094-S.

Feigenson, M.D., Carr, M.J., Maharaj, S.V., Juliano, S., and Bolge, L.L., 2004, Lead isotope composition of Central American volcanoes: Influence of the Galapagos plume: Geochemistry, Geophysics and Geosystems, v. 5, 14 p., doi: 10.1029/2003GC000621.

Gerlach, D.C., and Grove, T.L., 1982, Petrology of Medicine Lake Highland Volcanics: Characterization of end members of magma mixing: Contributions to Mineralogy and Petrology, v. 80, p. 147–159.

Goodfellow, W.D., Grapes, K., Cameron, B.I., and Franklin, J.M., 1993, Hydrothermal alteration associated with massive sulfide deposits, Middle Valley, northern Juan de Fuca Ridge: Canadian Mineralogist, v. 31, p. 1025–1060.

Grove, T.L., and Bryan, W.B., 1983, Fractionation of pyroxene-phyric MORB at low pressure: An experimental study: Contributions to Mineralogy and Petrology, v. 84, p. 293–309, doi: 10.1007/BF01160283.

Grunder, A.L., 1987, Low ^{18}O silicic volcanic rocks at the Calabozos caldera complex, southern Andes: Contributions to Mineralogy and Petrology, v. 95, p. 71–81, doi: 10.1007/BF00518031.

Harmon, R.S., and Gerbe, M.-C., 1992, The 1982–83 eruption at Galunggung volcano, Java (Indonesia): Oxygen isotope geochemistry of a chemically zoned magma chamber: Journal of Petrology, v. 33, p. 585–609.

Harmon, R.S., and Hoefs, J., 1995, Oxygen isotope heterogeneity of the mantle deduced from global ^{18}O systematics of basalts from different geotectonic settings: Contributions to Mineralogy and Petrology, v. 120, p. 95–114.

Hildreth, W., and Moorbath, S., 1988, Crustal contributions to arc magmatism in the Andes of Central Chile: Contributions to Mineralogy and Petrology, v. 98, p. 455–489, doi: 10.1007/BF00372365.

Hochstaedter, A.G., Ryan, J.G., Luhr, J.F., and Hasenaka, T., 1996, On B/Be ratios in the Mexican Volcanic Belt: Geochimica et Cosmochimica Acta, v. 60, p. 613–628, doi: 10.1016/0016-7037(95)00415-7.

Hunter, A.G., and Blake, S., 1995, Petrogenetic evolution of a transitional tholeiitic-calc-alkaline series: Towada volcano, Japan: Journal of Petrology, v. 36, p. 1579–1605.

James, D.E., 1981, The combined use of oxygen and radiogenic isotopes as indicators of crustal contamination: Annual Reviews of Earth and Planetary Science, v. 9, p. 311–344, doi: 10.1146/annurev.ea.09.050181.001523.

Kalamarides, R.I., 1984, Kiglapait geochemistry, VI. Oxygen isotopes: Geochimica et Cosmochimica Acta, v. 48, p. 1827–1836, doi: 10.1016/0016-7037(84)90036-X.

Kalamarides, R.I., 1986, High-temperature oxygen isotope fractionation among the phases of the Kiglapait intrusion, Labrador, Canada: Chemical Geology, v. 58, p. 303–310.

Kersting, A.B., Arculus, R.J., and Gust, D.A., 1996, Lithospheric contributions to arc magmatism: Isotope variations along strike in volcanoes of Honshu, Japan: Science, v. 272, p. 1464–1468.

LeMaitre, R.W., 1982, Numerical Petrology, Statistical Interpretation of Geochemical Data. Developments in Petrology 8: Amsterdam, Elsevier Scientific Publishing Company, 281 p.

Leeman, W.P., Carr, M.J., and Morris, J.D., 1994, Boron geochemistry of the Central American arc: Constraints on the genesis of subduction-related magmas: Geochimica et Cosmochimica Acta, v. 58, p. 149–168, doi: 10.1016/0016-7037(94)90453-7.

Macpherson, C.G., and Mattey, D.P., 1998, Oxygen isotope variations in Lau Basin lavas: Chemical Geology, v. 144, p. 177–194, doi: 10.1016/S0009-2541(97)00130-7.

Morris, J.D., Leeman, W.P., and Tera, F., 1990, The subducted component in island arc lavas: Constraints from Be isotopes and B/Be systematics: Nature, v. 344, p. 31–36.

Muehlenbachs, K., and Byerly, G., 1982, ^{18}O-enrichment of silicic magmas caused by crystal fractionation at the Galapagos spreading center: Contributions to Mineralogy and Petrology, v. 79, p. 76–79, doi: 10.1007/BF00376963.

Patino, L.C., 1997. Geochemical characterization of Central American subduction zone system: Slab input, output from the volcanoes, and slab-mantle interactions [Ph.D. thesis]: Piscataway, New Jersey, Rutgers University, 183 p.

Patino, L.C., Carr, M.J., and Feigenson, M.D., 1997, Cross-arc geochemical variations in volcanic fields in Honduras, C.A.: Progressive changes in source with distance from the volcanic front: Contributions to Mineralogy and Petrology, v. 129, p. 341–351, doi: 10.1007/s004100050341.

Patino, L.C., Velbel, M.A., Price, J.R., and Wade, J.A., 2003, Trace element mobility during spheroidal weathering of basalts and andesites in Hawaii and Guatemala: Chemical Geology, v. 202, p. 343–364, doi: 10.1016/j.chemgeo.2003.01.002.

Pokrovskii, B.G., and Volynets, O.N., 1999, Oxygen isotope geochemistry of extrusive rocks of the Kurile-Kamchatka arc: Petrology, v. 7, p. 223–245.

Sakuyama, M., 1981, Petrological study of the Myoko and Kurohime volcanoes, Japan: crystallization sequence and evidence for magma mixing: Journal of Petrology, v. 22, p. 553–583.

Sheppard, S.M.F., and Harris, C., 1985, Hydrogen and oxygen isotope geochemistry of Ascension Island lavas and granites: Variation with crystal fractionation and interaction with sea water: Contributions to Mineralogy and Petrology, v. 91, p. 74–81, doi: 10.1007/BF00429429.

Singer, B.S., O'Neil, J.R., and Brophy, J.G., 1992, Oxygen isotope constraints on the petrogenesis of Aleutian arc magmas: Geology, v. 20, p. 367–370, doi: 10.1130/0091-7613(1992)020<0367:OICOTP>2.3.CO;2.

Sisson, T.W., and Grove, T.L., 1993, Experimental investigations of the role of H_2O in calc-alkaline differentiation and subduction zone magmatism: Contributions to Mineralogy and Petrology, v. 113, p. 143–166, doi: 10.1007/BF00283225.

Smith, T.E., Thirlwall, M.F., and Macpherson, C.M., 1996, Trace element and isotope geochemistry of the volcanic rocks of Bequia, Grenadine Islands, Lesser Antilles arc: A study of subduction enrichment and intra-crustal contamination: Journal of Petrology, v. 37, p. 117–143.

Vroon, P.Z., Lowry, D., van Bergen, M.J., Boyce, A.J., and Mattey, D.P., 2001, Oxygen isotope systematics of the Banda arc; low δ^{18}O despite involvement of subducted continental material in magma genesis: Geochimica et Cosmochimica Acta, v. 65, p. 589–609, doi: 10.1016/S0016-7037(00)00554-8.

Walker, J.A., 1981, Petrogenesis of lavas from cinder cone fields behind the volcanic front of Central America: Journal of Geology, v. 89, p. 721–739.

Walker, J.A., Carr, M.J., Patino, L.C., Johnson, C.M., Feigenson, M.D., and Ward, R.L., 1995, Abrupt change in magma generation processes across the Central American arc in southeastern Guatemala: Flux-dominated melting near the base of the wedge to decompression melting near the top of the wedge: Contributions to Mineralogy and Petrology, v. 120, p. 378–390.

Walker, J.A., Roggensack, K., Patino, L.C., Cameron, B.I., and Matías, O., 2003, The water and trace element contents of melt inclusions across an active subduction zone: Contributions to Mineralogy and Petrology, v. 146, p. 62–77, doi: 10.1007/s00410-003-0482-x.

Woodhead, J.D., Harmon, R.S., and Fraser, D.G., 1987, O, S, Sr, and Pb isotope variations in volcanic rocks from the northern Mariana Islands: Implications for crustal recycling in intra-oceanic arcs: Earth and Planetary Science Letters, v. 83, p. 39–52, doi: 10.1016/0012-821X(87)90049-5.

Zindler, A., and Hart, S., 1986, Chemical geodynamics: Annual Reviews of Earth and Planetary Science, v. 14, p. 493–571, doi: 10.1146/annurev.ea.14.050186.002425.

Manuscript Accepted by the Society 19 March 2006